Volume 9, Number 1, 2015

Technical University of Cluj-Napoca
North University Centre of Baia Mare
Faculty of Engineering
Electrical. Electronic and Computer Engineering Department

Volume 9, Number 1, 2015

Carpathian Journal of Electrical Engineering

Carpathian Journal of Electrical Engineering

ISSN 1843 - 7583

UTPRESS PUBLISHER

TECHNICAL UNIVERSITY
OF CLUJ-NAPOCA

NORTH UNIVERSITY CENTRE OF BAIA MARE
FACULTY of ENGINEERING

ELECTRICAL, ELECTRONIC AND
COMPUTER ENGINEERING DEPARTMENT

Carpathian Journal of Electrical Engineering

Volume 9, Number 1, 2015
ISSN 1843 – 7583

http://cee.ubm.ro/cjee.html

CONTENTS

THE STUDY, DESIGN AND TESTING OF A LINEAR OSCILLATING GENERATOR WITH MOVING PERMANENT MAGNETS

Teodora Susana **OROS (POP)**[1], Ioan **BERINDE**[1], Radu **POP**[1]
[1] *Technical University of Cluj Napoca*
teodoraoros_87@yahoo.com

Keywords: linear oscillating generator, permanent magnet

Abstract: *This paper presents a study, design and testing of a Linear Oscillating Generator. There are presented the main steps of the magnetic and electric calculations for a permanent magnet linear alternator of fixed coil and moving magnets type. Finally it has been shown the comparative analysis between the linear oscillating generator with moving permanent magnets in no load operation and load operation.*

1. INTRODUCTION

A comprehensive presentation of the history, types and applications of linear electric actuators and generators was made by John Boldea in [1]. A new type of tubular linear permanent magnet generator for applications in convertorele wave energy was presented by Szabo et al. in. Note that applications of linear electric generators wave energy converters is restricted due to low frequency waves and large size of the resulting magnetic circuit at these frequencies.

Many more applications of permanent magnet generators are converters energy Stirling engines Piston free [2,3,4,5,6] .

Applications fixed frequency oscillating linear movement such as: compressors, pumps, vibrating or oscillating speakers using linear motors with permanent magnets, while Stirling engines or generators using thermal engines with linear oscillating piston. Linear oscillating electrical generators in combination with the free-piston Stirling engines have the following advantages over rotary generators:

- eliminates conversion of linear motion into rotary motion Stirling engine (crank system);
- structure is simpler;
- higher efficiency, especially in the operation of the resonance spring system;
- simplicity conditioning system of electricity generated by single-phase operation.

Oscillating linear generators can be classified into three main categories:

- linear oscillating generator with moving coil;
- linear oscillating generator with moving permanent magnets;
- linear oscillating generator with moving iron.

It will continue to study, design and test only of the linear oscillating generator with moving permanent magnets.

2. THE LINEAR OSCILLATING GENERATOR WITH MOVING PERMANENT MAGNETS

2.1. The design magnetic circuit of linear oscillating generator with moving permanent magnets

This alternator is of the synchronous type with excitation from the permanent magnets. From the figure 3 it can be seen that field line passes the air gap for two times, so the necessary magnetomotive force is:

$$F_{mm} = \frac{B_g}{\mu_0} \cdot 2 \cdot \delta = \frac{0{,}6}{4\pi \cdot 10^{-7}} \cdot 2 \cdot 1 \cdot 10^{-3} = 955A\,, \tag{1}$$

where:

B_g – magnetic flux density (B_g=0,6 T);

δ – the air gap lenght (δ=1 mm);

μ_0 – magnetic permeability of the air [H·m^{-1}, N·A^{-2}];

For the magnetization it was chosen two ring permanent magnets of the type EURONEOS 40x20x13.3, which have the properties presented in the table 1.

Table 1. The permanent magnets properties of the type EURONEO 3 40X20X13.3

Material	B_r *[T]*	H_c *[kA/m]*	BH_{max} *[kJ/m^3]*	*D [mm]*	*d [mm]*	*h [mm]*
N35	1.2	868	280	40	20	13.3

The magnetomotive force of the one magnet is:

$$F_{mm} = H_m \cdot h = H_C \cdot h = 868 \cdot 0{,}0133 = 11{,}54kA. \tag{2}$$

Can be seen that 11,54 kA=11540 A>955 A, therefore, the magnets were chosen correctly.

2.2. The coil design of linear oscillating generator

The indus coil design will be made according to the voltage that is aimed to be induced in the coil. We considered an induced voltage at 10 Hz frecvency of U=18 V_{ef} voltage. The magnetic flux by this coil varies between + Φ_{max} and -Φ_{max} so that the magnetic flux variations:

$$\Delta\Phi = \Phi_{\max} - \left(-\Phi_{\max}\right) = 2\Phi_{\max} = 2B_m A_m . \quad (3)$$

The permanent magnet area is:

$$A_m = \frac{\pi\left(D^2 - d^2\right)}{4} = \frac{\pi\left(40^2 - 20^2\right)}{4} \cdot 10^{-6} m^2 = 942 \cdot 10^{-6} m^2. \quad (4)$$

Now, the magnetic flux variation is:

$$\Delta\Phi = 2B_m \cdot A_m = 2 \cdot \frac{B_r}{2} \cdot A_m = B_r \cdot A_m = 1{,}2T \cdot 942 \cdot 10^{-6} m^2 = 1130 \cdot 10^{-6} Wb. \quad (5)$$

The turn voltage is:

$$e = \frac{\Delta\Phi}{T} = f \cdot \Delta\Phi = 50Hz \cdot 1{,}13 \cdot 10^{-3} Wb = 56{,}5 \cdot 10^{-3} V / spir\check{a}\,, \quad (6)$$

considering f=50Hz from mechanical design stage.

For a voltage of U=24Vef we will need:

$$N = \frac{\sqrt{2} \cdot U}{e} = \frac{\sqrt{2} \cdot 24}{56{,}5 \cdot 10^{-3}} = 600\ spire. \quad (7)$$

The magnetic circuit window where the coil is placed has the area:

$$A_f = a \cdot b = 20 \cdot 29 = 580 mm^2. \quad (8)$$

The coil conductor cross-section area is:

$$s_C = \frac{A_f \cdot k_1}{N} = \frac{580 \cdot 0{,}4}{600} = 0{,}36 mm^2\,, \quad (9)$$

where: k_1 – is the winding (k_1=0,4).

Now we can calculate the fixed coil conductor diameter:

$$d_C = \sqrt{\frac{4 \cdot s_C}{\pi}} = \sqrt{\frac{4 \cdot 0{,}36}{\pi}} = 0{,}6mm. \quad (10)$$

Figure 2 shows the fixed coil of linear oscillating generator with moving permanet magnets designed and developed.

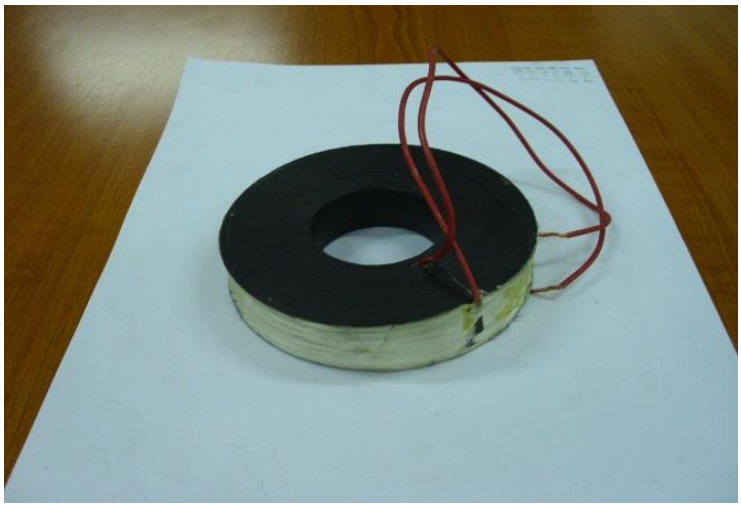

Fig. 2 The fixed coil of linear oscillating generator with moving permanent magnets

3. TESTING OF LINEAR OSCILLATING GENERATOR WITH MOVING PERMANENT MAGNETS

Figure 3 shows the linear oscillating generator with moving permanent magnets, development and fixed on test bech.

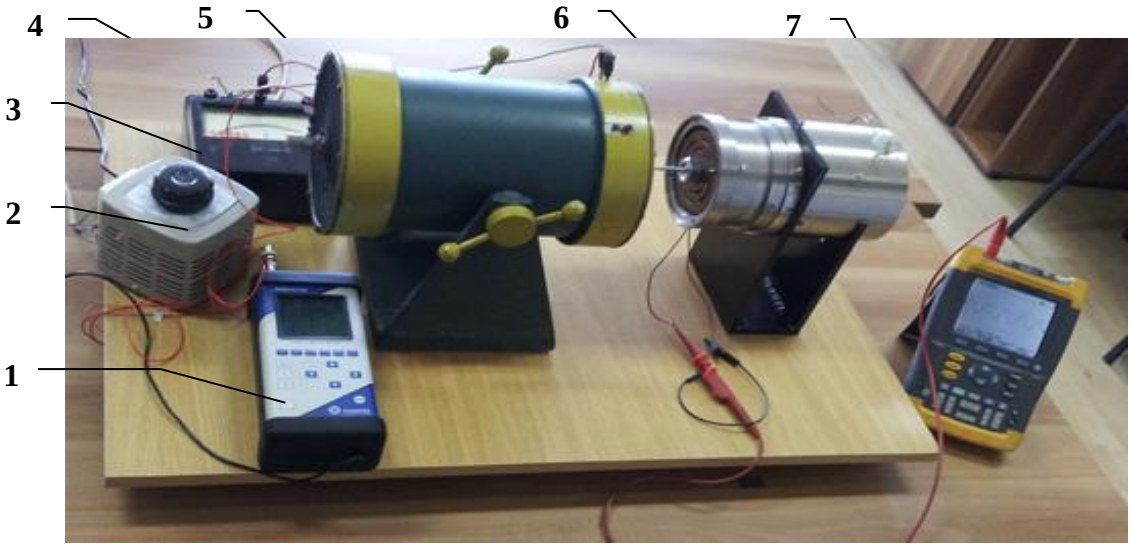

Fig. 3 Test bench of linear oscillating generator with moving permanent magnets:
1 – vibrometer, 2- autotransformer, 3 – ampermeter, 4 – vibration sensor, 5 – vibrator VEDP-10, 6 – linear oscillating generator with moving permanent magnets, 7 - oscilloscope Fluke 196.

3.1. The resonance oscillating frequency checking

It hit with a hammer the moving equipment of linear oscillating generator with moving permanent magnets and it hah been in free vibrations which induced in the fixed coil

a signal damped voltage (see figure 4). This signal was viewed with Fluke 196 digital oscilloscope.

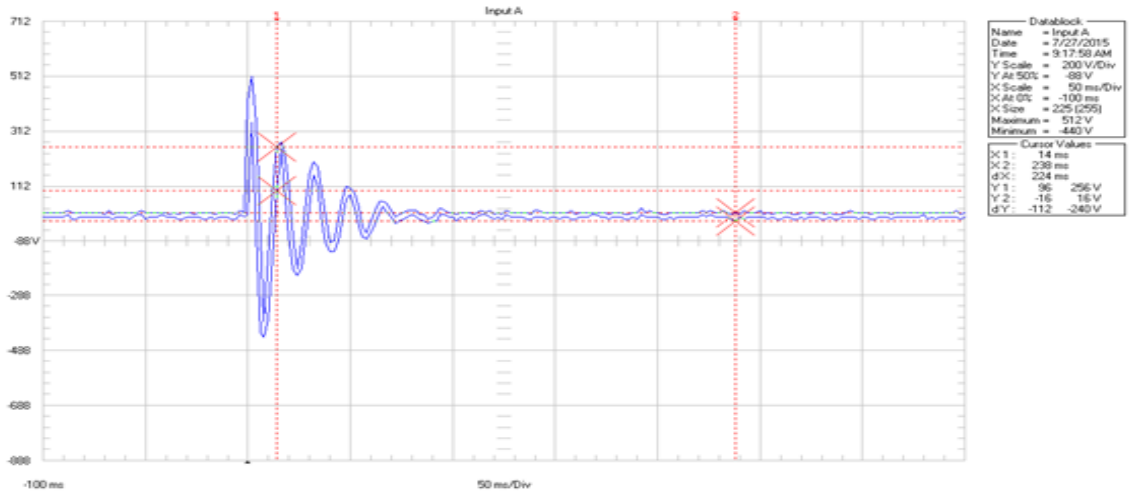

Fig. 4 Free oscillations of linear generator with moving permanent magnets

In this figure can see that the distnace in time between two peaks of oscillation is 18 ms, which corresponds to the frequency of 55,5 Hz, similar to taken as a given design (50 Hz).

3.2. The testing of linear oscillating generator with moving permanent magnets driven by vibrator VEDP-10

Figure 5 shows the answer of linear oscillating generator with moving permanent magnets driven by vibrator VEDP-10 in load operation with a frequency 50 Hz and vibration amplitude A=3 mm. This answer has been counted by the Fluke 196 oscilloscope.

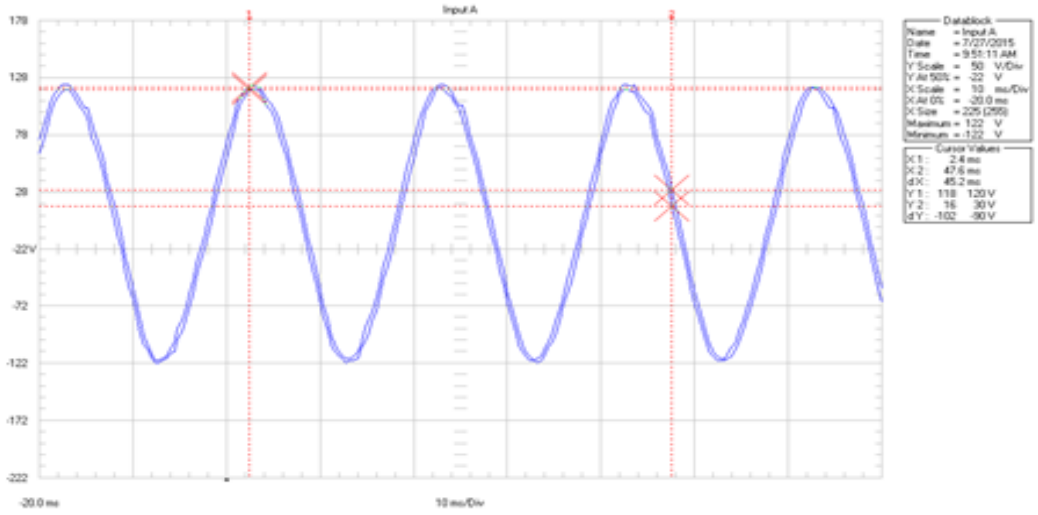

Fig. 5 Sinusoidal oscillations of linear generator with moving permanent magnets

So, we can see that generated alternating voltage amplitude is 122 V respectively 86 V_{ef}. This high value, is much higher than the amount considered design (24 V_{ef}). This thing is due to the large number of turns of the coil fised and because the two permanent magnets of moving equipment, which it was of very good quality and functioning almost resonance oscillating system.

Also, with Fluke 196 digital oscilloscope an analysis was made sinusoidal harmonic voltage generated by the linear oscillating generator with moving permanent magnets and the results is shown in figure 6.

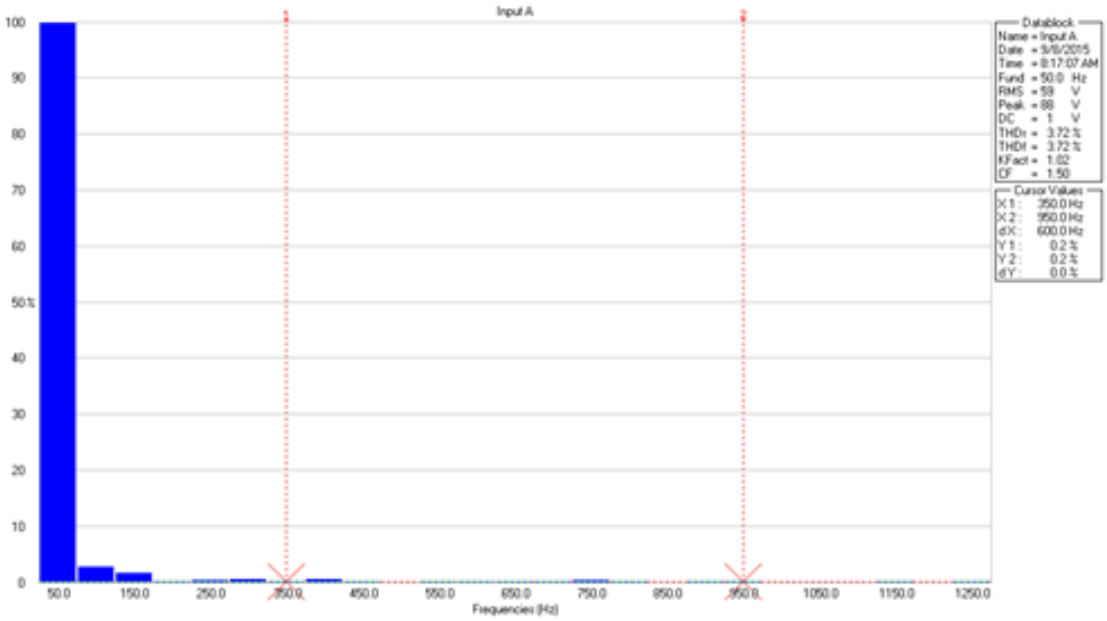

Fig. 6 Harmonic analysis of voltage generated by linear oscillating generator with moving permanent magnets

We can see that the voltage generated has a important harmonic of second snd third order, and the THD is 3,72%, which confirms the finding visual on voltage generated.

3.3. The testing of linear oscillating generator with moving permanent magnets driven by vibrator VEDP-10 in load operation

Figure 7 shows the test bench of linear oscillating generator in load operation with moving permanent magnets.

Figure 8 shows the answer of the linear oscillating generator with moving permanent magnets in load operation. This answer has been counted by the Fluke 196 oscilloscope.

We can see that this value of 7,2 V_{ef} is less than 24 V_{ef} was taken as the design. This is explained by the fact that the vibration of amplitude (2 mm) was less than the nominal amplitude of 5 mm. Also, we can see that the voltage generated has decreased a lot in load operation.

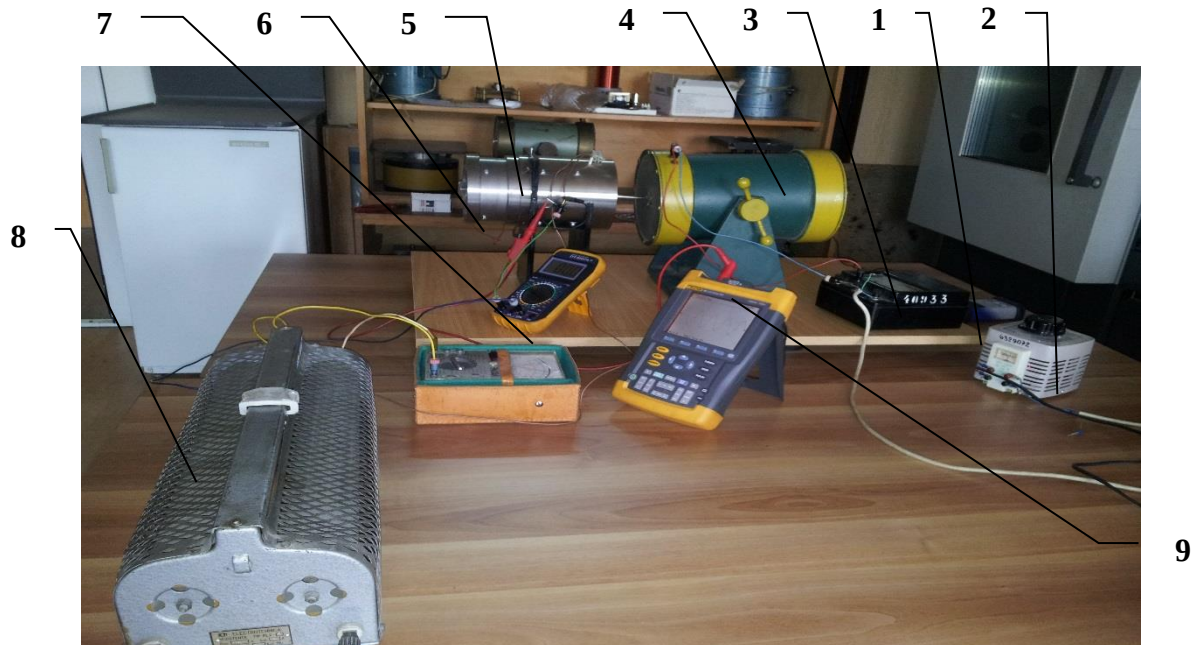

Fig. 7 Test bench of linear oscilating generator in load operation:

1 – vibrometer, 2- autotransformer, 3 – ampermeter, 4 – vibrator VEDP-10, 5 – linear oscillating generator with permanent magnets; 6 –ampermeter of load, 7 –voltmeter of load, 8 – load R_s=50 Ω;
9 - oscilloscope Fluke 196.

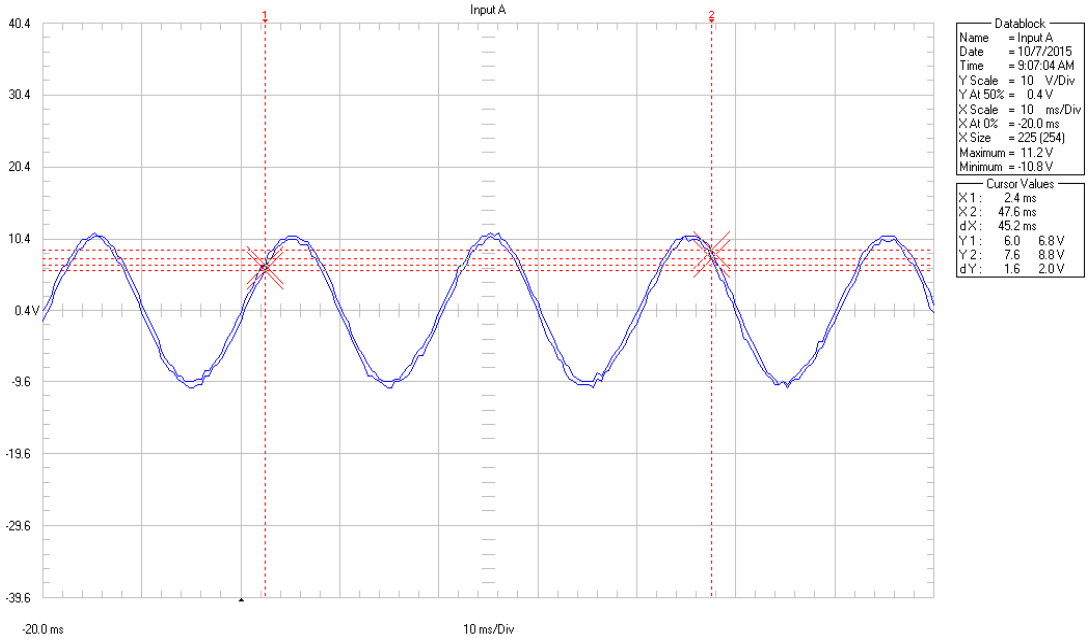

Fig. 8 The test of linear oscillating generatorwith on a load resistance R_s=50 Ω

Figure 9 shows the spectral analysis of voltagew generated by the linear oscillating generator with moving permanent magnets in load operation.

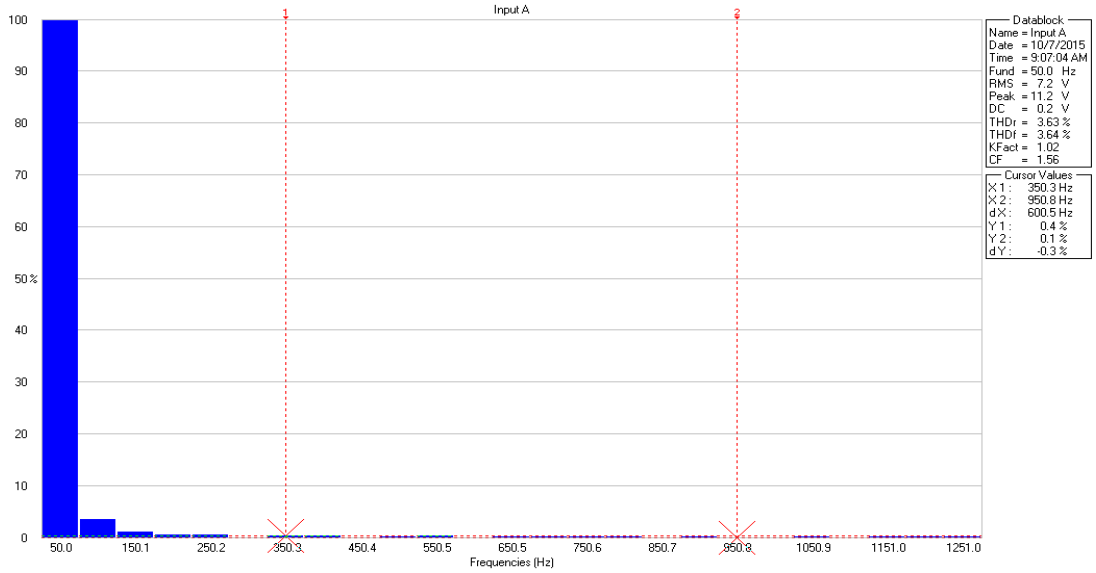

Fig. 9 Spectral analysis of voltage generated by the linear oscillating generator in load

Se observă că sarcina funcționează ca un filtru de armonici, deoarece coeficientul de distorsiune THD s-a redus de la 3,72% în gol la 3,63% în sarcină.

3.4 Measuring magnetic induction in the air gap of the linear oscillating generator

It was used for measuring a teslametru with Hall probe, which probe has been inserted ito the gap through the recesses of the membrane spring ina position pressed by 5 mm of the mobile equipment. The measured value was 0,57 T very close value of the design data 0,6 T and the magnetic field calculated by method analytical of reluctance (0,57,T) and the finite element method.

4. COMPARATIVE ANALYSIS OF A LINEAR OSCILLATING GENERATOR WITH MOVING PERMANENT MAGNETS IN NO LOAD AND IN LOAD OPERATION

Based on results of these tests can be compared between the linear oscillating generator with moving permanent magnets in no load and in load operation. This was the main objective of this paper. In the table 1 we can see the comparative analysis of linear oscillating generator in no load and in load operation.

LINEAR OSCILLATING GENERATOR WITH MOVING PERMANENT MAGNETS	
in no load operation	**in load operation**
➢ The voltage generated in no load operation is 86 V_{ef} is higher than 24 V_{ef} taken as a design data;	➢ The voltage generated in load operation 7.2 Vef is less than 24 Vef taken as a given design, which is

➢ The cogging force present, which on the vibration amplitude small (2 mm) much smaller than the polar pich (14 mm) increases the strength of the excitation vibrators; ➢ Wave voltage has not a sinusoidal waveform THD=3.72% pure, ➢ In terms of technology requires permanent magnets easier and cheaper;	explained by the fact that the amplitude of vibration (2 mm) was less than 5 mm nominal amplitude; ➢ In load operation load coefficient = 3.63% THD distortion is less than 3.72% THD = empty, because the task acts as a harmonic filter;

5. CONCLUSIONS

In this paper was designed and testes a linear oscillating generator with moving permanent magnets. The ring-shaped iron rotor with the rare earth axially magnetized permanent magnets is used as magnetic pole of the mover, because in the case of symmetric structure the leakage magnetic flux is smaller than that of the flat type one. Also, the mass of the copper coil is less than that in the case of flat-type generator because there is no end coil.

It tested the resonance frequency of the oscillating linear generator system of mobile permanent magnet mobile and obtained a value close to the value of 55.5 Hz 50 Hz proposed as the date design.

It has been tested under load oscillating magnet linear generator mobile driven by electrodynamic shaker VEDP-10, excited by sinusoidal vibration amplitude 2 mm. The voltage generated was 7.2 Vef slightly less than 24 Vef was taken as design time, although the amplitude of vibration of the drive was only 2 mm less than the nominal 5 mm. This was found for the following reasons: the effect of a positive reaction force for the teeth of the vibration amplitudes below 5 mm. This was proven by calculating the force profile teeth finite element giving a maximum of 30 N at z = 5 mm, similar motive value.

Finally it was made a comparison between the linear oscillating generator with moving permanent magnets in no load and in load operation.

ACNOWLEDGMENT

This paper is supported by the Sectorial Operational Programme Human Resources Development (SOP HRD), ID/134378 financed from the European Social Fund and by the Romanian Government.

REFERENCES

[1]. I Boldea, 2013 *Linear Electric Machines, Drives, and MAGLEVs Handbook*, CRC Press, Taylor&Francis Group, London 2013.

[2]. J. Wang and D. Dowe, "A Linear Permanent Magnet Generator for a Free-Piston Energy Converter", Conference on Electric Machines and Drives, 2005 IEEE International, pp. 1521 – 1528, 15-15 May 2005.

[3]. M. W. Arshad et all, 2004 "Use of Tranverse Flux Machines in a Free-Piston Generator", IEEE TRANSACTIONS ON INDUSTRY APPLICATIONS, Vol. 40, No. 4, pp. 1092-1100, July/August 2004.

[4]. W. Beale, *"Stirling Engines for Developing Countries"*, U.S. National Academy of Sciences, Energy for Rural Development, 1981.

[5]. Johnson E. and Pickard D., "Application of 1 kWe Free-Piston Stirling Engine to Mobile Cogeneration", 3rd International Energy Conversion Engineering Conference, 15-18 August 2005, San Francisco, California, 2005.

[6]. R. Mikalsen, P. A. Roskilly, *"The Control of a Free-Piston Engine Generator. Part 1: Fundamental Analyses"*, Science Direct, Applied Energy 87 (2010) 1273-1280, ELSEVIER, 2010.

OPERATION OF WIND FARMS TO DEFECTS IN THE MEDIUM VOLTAGE GRID

Ioan **BERINDE**[1], Teodora Susana **OROS (POP)**[2]

[1,2] *Technical University of Cluj-Napoca, Romania, Faculty of Electrical Engineering, Department of Power Engineering and Management, Memorandumului 28, 400114, Cluj-Napoca, Romania*

ioan_berinde@yahoo.com,

Keywords: Wind Farm, Medium Voltage

Abstract*: Integrating wind power in medium voltage networks raise problems both economic and technical. The article presents a wind power plant integration in a medium voltage network and its operation in case of fault on other section than the line that wind power plant inject power. In the wind power plant is connected and compensator STATCOM for reactive power compensation. The wind power plant is equipped with squirrel cage induction generators.*

1. INTRODUCTION

Connecting wind farms to electricity grids requires solving a large number of technical problems to achieve safe operation of these sources in the electricity system presence and maintaining the system into operation in their presence.[1]

Power groups used in the wind power plants are of two categories, depending on the speed control: Fixed speed and variable speed. Fixed speed turbine is the oldest type of turbine. Train squirrel cage induction generator that connects directly to the grid.[1]

Wind turbine with fixed speed

This configuration is known as the "Danish concept" that uses a squirrel cage induction generator (GARS) to convert mechanical energy into electrical energy. Because of the difference between the turbine rotor speed and rotor speed asynchronous generator is necessary to use a multiplier (gearbox) that perform the necessary harmony between these two

speeds. Slipping asynchronous generator varies little as the generated power increases, without being kept constant. Since the electric machine speed variations are less than 1%, this turbine is considered to operate at a constant speed or fixed speed [2,3].

The turbine fixed speed is now fitted with brake active aerodynamics (stall control) even though they were designed and turbine systems with fixed speed and adjusting the angle of attack, asynchronous generator with squirrel-cage rotor is connected to the grid through an transformer. Because of voltage fluctuations, asynchronous generator absorbs reactive power from the grid. This is why using a capacitor battery with the role of reactive power compensator. Connecting to the network is achieved through a soft starter having the role to prevent inrush currents when the coupling conditions along the two power sources (asynchronous generator and network) are not satisfied.[4,2]

Whatever the method to control power generated, it should be noted that fluctuations of wind speed are transformed into mechanical power fluctuations and as a consequence into electrical power fluctuations. For a small grid, these electrical power fluctuations give rise to variations in the voltage at the point of grid connection. The main disadvantage of this configuration is that it requires a system of control (adjustment) of the speed, a strong grid, and must be able to withstand considerable mechanical stress [4.2].

In almost all cases, the internal networks of medium voltage or high voltage of wind power and photovoltaic and in some cases even power lines connecting these central power system are made of electrical cables that generate significant quantities of reactive power which influences power factor into PCC. In these circumstances it is necessary compensation of reactive power for voltage at the PCC and reactive power exchange with the grid of the power system to meet the requirements of technical codes electricity transmission grid or distribution of electricity [5].

Modern solutions for rapid and automatic voltage control and fluctuations of energy use electronic control systems for reactive power flow. Systems FACTS (Flexible Alternating Current Transmission System) built based on power electronic circuits, ensure state control of electrical quantities to achieve the necessary transfer of power in electricity grids. [5]

1.1. Static synchronous compensator shunt (STATCOM)

It is a device that uses power electronics with forced commutation (eg GTO - Gate turn-off thyristor, IGBT - insulated gate bipolar transistors) to control voltage and power flow, and improving the transient stability into electricity grids. STATCOM uses a voltage source converter to absorb or inject in nodes grid is connected amount of reactive power to control voltage in node connection or flow control reactive on power line connection at the power system [6].

STATCOM is the most efficient synchronous compensator shunt, his answer is the same as the synchronous compensators (rotating) and, moreover, has no mechanical inertia. The three-phase schematic diagram is shown in Figure 1 [6].

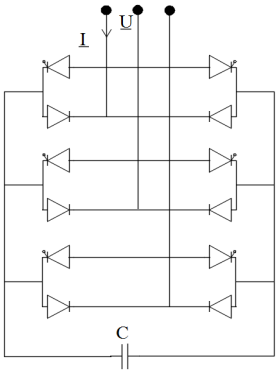

Fig.1- Three-phase scheme of STATCOM

A STATCOM can be used in two ways [7]

a) *The voltage control mode connection.*

STATCOM regulates voltage into the mains connection point by controlling the reactive power absorbed or injected into the power grid through a converter VSC. Reactive power absorbed or injected into the grid by this device depends on the voltage amplitude in the connection point. When the voltage amplitude into the connection point is higher than the reference value (Uref), STATCOM absorbs reactive power from the grid and thus reduce the tension in the connecting node (comparison inductive STATCOM). When the voltage amplitude into their grid connection point is lower than the reference value (Uref), STATCOM inject reactive power into the power grid and thus there is an increase in tension in the node grid connection (comparison capacitive STATCOM)

b) *Reactive power control mode in the connection node*

In this mode of operation is controlled STATCOM reactive power output, independent of other parameters of grid.

1.2. Protection of medium voltage grid

The primary aim of energy system is to generate, transport and distribute electricity to consumers. Reaching the goal requires both appropriate equipment reliability primary and secondary protective equipment and automation taking economic factors into account.

Ensuring uninterrupted operation of the electrical system is of great importance, both because the consequences can be serious disruptions in operation, and that electrical installations are more exposed to disturbances than other types of installations. The gravity of the consequences derived primarily from the fact that - part electrical installations generally a complex energy system - a fault appeared in a place disturbing normal functioning of the whole system; Second, the severity of defects in electrical installations due to very high

energies that interfere into their development, leading to extremely high destructive effects.. Knowing the methods of intervention and detection of these defects have developed various protective equipment to cover most conditions from damages that may arise in their functioning.

In general, medium voltage lines are fitted with the following types of protection:[8]

a) Timed overcurrent protection against phase defects

$$I_{maxII}=k_{sig}\cdot I_{sarc.max} \quad (1)$$

In which:

- $I_{sarc.max}$ it is the maximum current that can be carried by a medium voltage line limited by the diameter or type current transformer existing supply end;
- K_{sig} is a safety factor equal to 1,25 ÷ 1,3

b) Instantaneu overcurrent protection (cutoff current)

$$I_{maxI}=k_{sig}\cdot I_{scc.max} \quad (2)$$

In which: - $I_{scc.max}$ is three phase short-circuit current calculated at the end of the line for which the adjustment protection;

- K_{sig} is a safety factor equal to 1,25 ÷ 1,3

c) Timed current homopolar protection

$$I_{hII}=k_{sig}\cdot \varepsilon\%/100\cdot I_{nTC} \quad (3)$$

In which:

- I_{nTC} is the nominal primary current of the transformer current with which is made Holmgren the filter
- K_{sig} is a safety factor equal to k_{sig}=1,5

1.3 Wind farm protections

To protect wind power plant, against defects that might arise in their grid and beyond, wind power plants must be equipped with a minimum of protection [9]:

- Instantaneu overcurrent protection (cutoff current)
- Timed overcurrent protection against phase defects
- minimum frequency protection
- maxim frequency protection
- minim voltage protection
- maxim voltage protection
- protection against phase asymmetry..

As noted they represent a minimum and may be supplemented with other protection according to the specific network which supplies.

1. *Minimum and maximum frequency protections*

Minimum and maximum frequency protections are designed to protect wind farm against isolated operation and so as not cause defects aggravation of the grid are connected.

Recommendations standards in force for minimum and maximum frequency protections are:

$$f_{min} = 47Hz, t = 0.5s \quad (4)$$

$$f_{max} = 52Hz, t = 0.5s \quad (5)$$

1. Minimum and maximum voltage protections

The purpose of this protection is to protect generator against minimum / maximum voltage that could occur, and protect network against overvoltage created by the wind power plants. Protection can be used as short circuit protection because fault current increases during what has the effect of lowering the minimum voltage and starting minim voltage protection of generator, and after the set time the control tripping protected equipment

To have clarity on the parameters (voltage) so protection is supplied from groups as the bars of medium voltage point of common coupling. Minimum and maximum voltage protections have two stages:

a) step of signaling

$$U_{max} = +6\%, t < 60s \quad (6)$$

$$U_{min} = -6\%, t < 60s \quad (7)$$

b) tripping stage

$$U_{max} > +10\%, t \le 0.3s \quad (8)$$

$$U_{min} < -10\%, t \le 0.3s \quad (9)$$

2. Overcurrent protection

Protection as a value adjustment has two steps:

a) Delayed step – against overcurrent occurring in connecting wind groups with a lower power and greater control over.

b) Rapid step – current cutoff – against short circuits in the internal grid of the wind farm with a higher current value and time t = 0s

Setting values for the two steps, to meet current standards must be set so fast maximum protection to eliminate defects in the 0s, the recommended value is $I_{max\,I} = 10 \cdot I_{nom}, t = 0s$, and timed overcurrent protection is sufficiently sensitive against overloads caused by the connection groups, but at the same time, selective to allow groups to remain in service to transient grid faults., recommended value is $I_{max\,II} = 1.1 \cdot I_{nom}, t \le 1.5s$

3. Protection against asymmetries between phase and earth

Protection has a simple operating principle verifying increased or decreased voltage on phase is also adjusted in two steps, one signal and another tripping.

a) *Asymmetries* <±5% , t=10s - signalization

b) *Asymmetries* ≥±5% , t=1s - trip

2. SIMULATION AND DISCUSSION

Simulations were performed using Matlab - Simulink. The proposed grid simulation is composed of a wind power plant with an installed power of P = 9 MW, which supplies by a 20 kV line, with a length of 5 km, into substation St.A.

St. A. is composed of a transformer Un=110/20 kV, Sn = 25 MVA. Short circuit power Sk, on the 110 kV bar is Sk=2000 MVA. On the line connecting the wind power plant and substation St.A. is connected a line that supplies the consumer with a power of P = 500 kW.

The wind power plant is composed of 6 units of 1.5 MW each. The wind power plant is equipped with squirrel cage induction generators and synchronous compensator shunt STATCOM 3MVAR

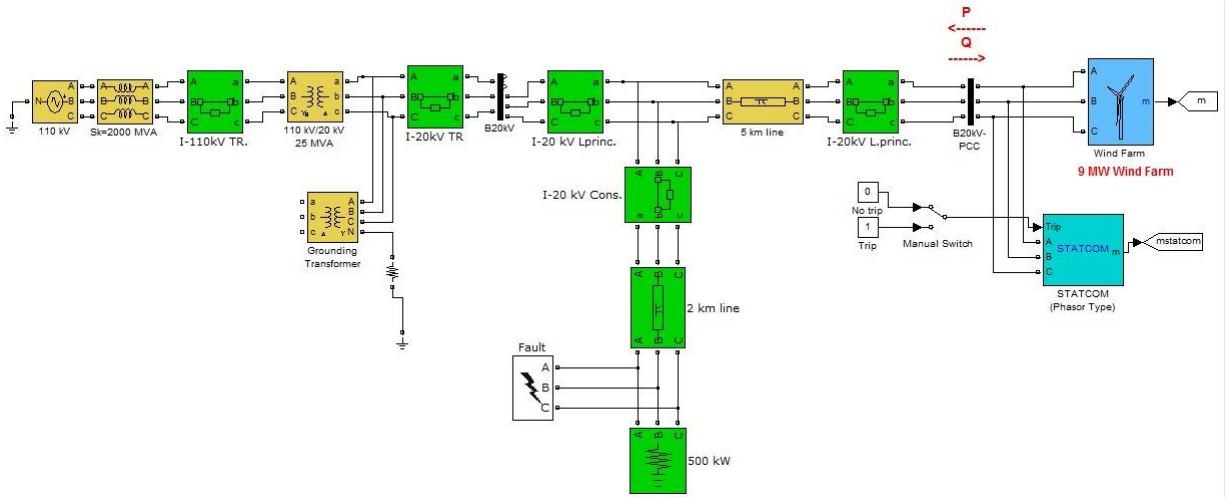

Fig.2 – The proposed grid simulation

A. Determination protections settings.

For simulated grid were adjusted the protections:

L 20 kV –principal

a) Instantaneu overcurrent protection

$$I_{maxI} = k_{sig} \cdot I_{sccmax} = 1.1 \cdot 3555A = 4000A - t = 0.2s$$

b) Timed overcurrent protection

$$I_{max\,II} = k_{sig} \cdot I_{sarc.max} = 1.2 \cdot 325 = 390A - t = 1s$$

Where: $I_{sarc..max}$ – is the maximum current that can be transported safely on line (Imax = 325 A- limited by conductor cross section OL-Al 95 mm^2)

c) Homopolar current protection

$$I_{hII} = k_{sig} \cdot \frac{\varepsilon\%}{100} I_{nTC} = 1.5 \cdot \frac{5}{100} \cdot 400 = 30A - t = 0.2s$$

L 20 kV – The consumer 1

a) *Instantaneu overcurrent protection*

$$I_{max\,I} = 1000 - t = 0s$$

b) *Timed overcurrent protection*

$$I_{max\,II} = 100A - t = 0.5s$$

c) *Homopolar current protection*

$$I_{hII} = 20A - t = 0s$$

Wind power plant

Adjusted values respectively measures for protection of minimum and maximum voltage of 20kV bar from point of common coupling are expressed on a per unit. So it is necessary to choose a basic voltage Ub and voltage that wind power works at one time called the current value and noted with U_C:

$$U_b = 21kV\,;\, U_C = 21kV\,;\, U_{u.r.} = \frac{U_C}{U_b} = \frac{21}{21} = 1u.r.$$

a) Instantaneu overcurrent protection directed towards the wind farm

$$I_{max\,I} = 10 \cdot I_{nom} = 10 \cdot 260 = 2600A - t = 0s$$

b) Timed overcurrent protection directed towards the wind farm

$$I_{max\,II} = 1.4 \cdot I_{nom} = 1{,}4 \cdot 260 = 360A - t = 1.5s$$

c) Minimum voltage protection

$$U_{min} = 0.7p.u. = 0.7 \cdot 21 = 14.7kV \text{ -for line voltage}$$

$$U_{min} = 0.7p.u. = 0.7 \cdot 12 = 8.4kV \text{ - for phase voltage}$$

d) Maxim voltage protection

$$U_{max} = 1.1p.u. = 1.1 \cdot 21 = 23.1kV \text{ - For line voltage}$$

$$U_{max} = 1.1p.u. = 1.1 \cdot 12 = 13.2kV \text{ - For phase voltage}$$

e) Protection against voltage asymmetry 5% - t=1s

f) Protection of minimum frequency

$$f_{min} = 47Hz - t = 0.5s$$

a) Protection of maxim frequency

$$f_{max} = 52Hz - t = 0.5s$$

B. Making simulation

It will simulate the operation of the grid in normal operating conditions without any fault on the grid and without connecting consumer 1-500 kW.

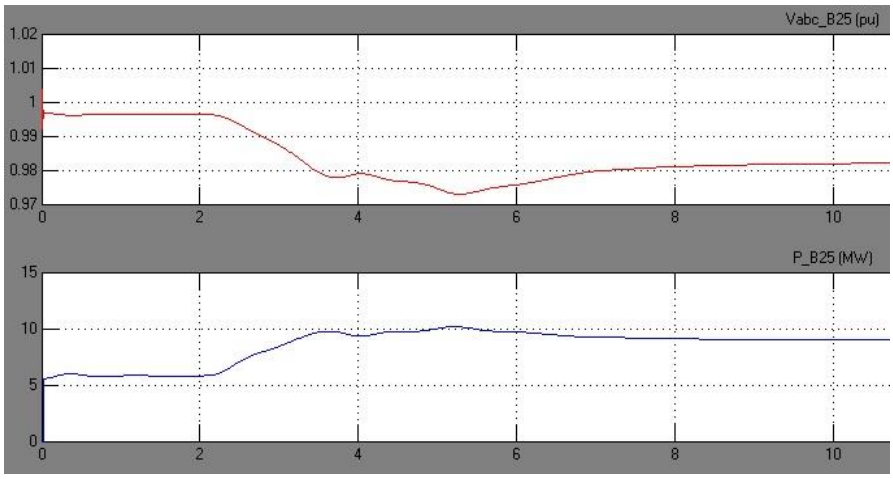

Fig.3 – Functioning of the grid with STATCOM connected

As you can see in Figure 3 with static compensator shunt - STATCOM connected voltage on bar 20 kV in the wind power plant (V_B25) has a value of 0.98 pu - 11.99 kV (20.75 kV), active power (P_B25) amounts to 9 MW.

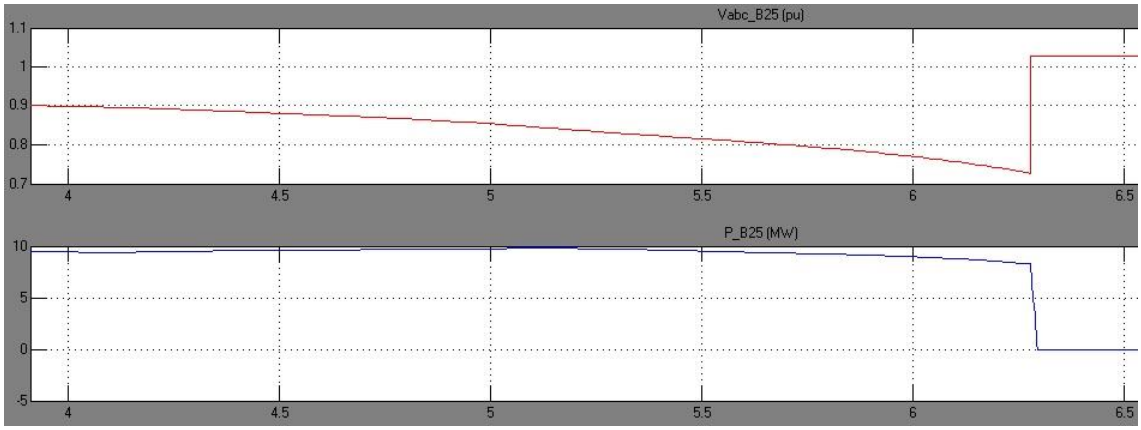

Fig.4 – Functioning of the grid with STATCOM disconnected

If disconnection static compensator shunt - STATCOM, a part of the reactive power required asynchronous generators is produced locally by capacitor banks' own plant, while the remaining reactive power required producing full active power assets by groups wind is consumed from the 20 kV grid. Increased consumption of reactive power from grid has the effect of lowering of voltage bar 20 kV corresponding point of common coupling (PCC) - the measure Vabc_25 (pu) under value with adjustment for the protection of minimum voltage of wind units (Umin = 0,7p.u -8.4 kV t = 0.1s) which has the effect of tripping all groups of wind power by 0.1s at the time t = 6,3s. Once tripping the wind groups, voltage on bar 20 kV corresponding PCC returns to the value of 0.988 p.u., the bar remaining energized, fed from 20 kV grid.

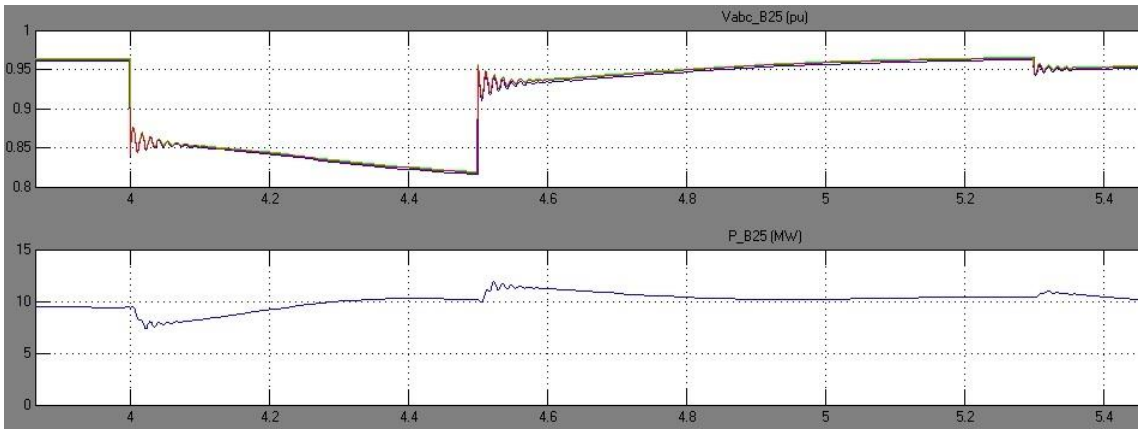

Fig.5 – Three phase fault on the line that supplies consumer 1-500 kW

At time t = 4s there is a three phase fault in the L- 20 kV which supplies the consumer 1. When the fault occurred which lasts 0.7s, whose value is approximately 700A, starts timed overcurrent protection corresponding consumer 1, after 0.5s (4,5s) give the command to trip I-20kV which supplies consumer 1. The fault is removed by tripping I 20 kV which supplies consumer 1. In RAR pause (0,8s) the arc extinguishes and after tripping, 0,8s connects at I 20kV for the consumer 1 (5,3s). It can be seen that the emergence fault, the voltage on bar 20 kV corresponding wind farm (B_25) decreases the value 0,976pu - 11.85 kV (20.5 kV) to the value of 0.83 p.u. - 10.1 kV (17.43 kV - 4,5s), but wind power plant remains connected because value required and setting for the minim voltage protection of wind turbine voltage is 0.7 pu - 8.4 kV (14.7 kV).

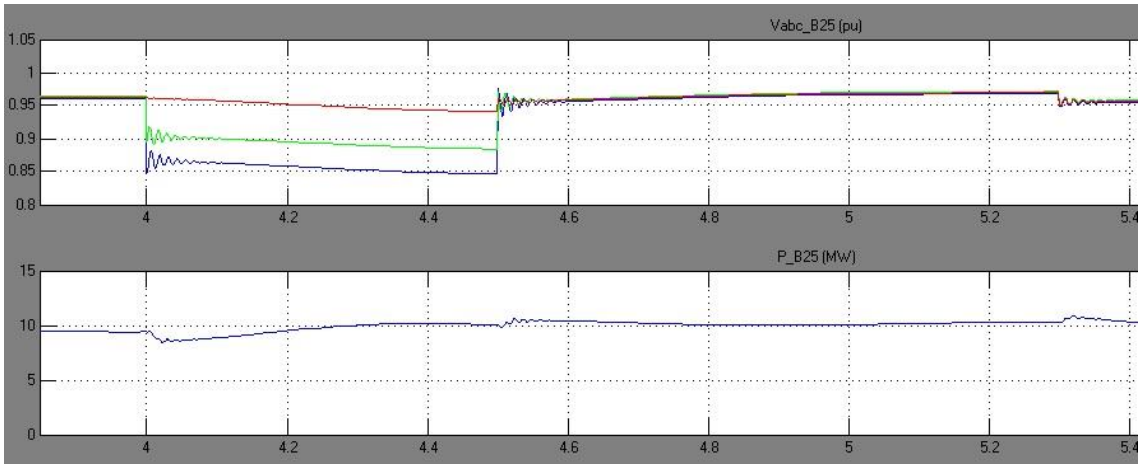

Fig.6 – Phase to phase fault on the line that supplies consumer 1-500 kW

Was simulate a phase-phase short circuit R-S, with a current of 600 A, fault notified by the overcurrent protection of consumer timed 1.

At t = 4s take place phase to phase fault R-S, with a value of I = 600 A. Started timed overcurrent protection after 0.5s and tripping the switch of the Consumer 1 (tripping all three phases). The defect is removed, the voltage 20 kV bar corresponding PCC increase to an

amount above 0,95p.u. After 0,8s from the eliminate defects by tripping breaker for the consumer, RAR automation connects the switch and the consumer1 continues to be powered.

3. CONCLUSIONS

Choosing right protections settings in medium voltage grid is very important. Defects which were not removed from the sections where defects have taken place may tripping the upstream elements and has the effect of tripping line that debits the wind power plant. In case of squirrel cage asynchronous generators, it is very important that the entire reactive power needed to be produced locally. Disconnection STATCOM device of wind power plant has the effect of tripping groups by under voltage protection. Squirrel cage induction generators of wind power plant consumes reactive power from the grid that has as effect on lowering voltage on the medium voltage bar below setting of minimum voltage protections groups. For any defect appeared radial section and removed the protections own defective equipment, wind power plant remains in operation.

ACNOWLEDGMENT

This paper is supported by the Sectoral Operational Programme Human Resources Development POSDRU/159/1.5/S/137516 financed from the European Social Fund and by the Romanian Government

REFERENCES

[1]. M. Mihăiescu, I. Folescu și C. Toader, „Cerinte de conectare și functionare pentru centralele eoliene," în *Forumul Regional al energiei - FOREN*, Neptun, 2010

[2]. AG-Siemens, „Safety and protection for wind turbines," Regensburg, 2012.

[3]. B. Ioan, O. S. Teodora și B. Horia, „Study about the Reactive Power of the Overhead Power Lines High Voltage," Baia Mare, 2014.

[4]. T. EL-Fouly și M. Salama, „Voltage Regulation of Wind Farms Equipped with variable-Speed Doubly-Fed Induction Generators Wind Turbine," *IEEE*, pp. 1-8, 24-28 June 2007.

[5]. F. Vatră și D. Ilișiu, „Condiții tehnice de racordare a centralelor eoliene la rețelele electrice ale SEN. Comparatie între diferite coduri din Europa," în *Conferinta Nationala și Expozitia de Energetică*, Sinaia, 2009.

[6].P. Postolache, „Compensatoare sincrone și compensatoare statice," în *SIER*, București, 2012.

[7]. J. Agrawal, K. D. Joshi și V. K. Chandrakar, „Experimental study of thyristor controlled reactor (tcr) and gto controlled series capacitor (GCSC)," 2011.

[8]. Electrica, „Îndreptar pentru proiectarea rețelelor de medie tensiune cu neutrul legat la pământ prin rezistență," ICEMENERG, București, 2014.

[9]. Abdulhadi , X. Li și F. Coffele, „International White Book on DER Protection: Review and Testing Procedures," Department of Electronic and Electrical Engineering University of Strathclyde, Glasgow, 2011.

[10]. http://www.mathworks.com/

INDUCTIVE COUPLING BETWEEN OVERHEAD POWER LINES AND NEARBY METALLIC PIPELINES. A NEURAL NETWORK APPROACH

Levente **CZUMBIL**, Dan Doru **MICU**, Denisa **ȘTEȚ**, Andrei **CECLAN**
Dep. of Electrotechnics and Measurement, Technical University of Cluj-Napoca, Romania
levente.czumbil@ethm.utcluj.ro

Keywords: electromagnetic compatibility, electromagnetic interference, finite element methods, neural networks, pipelines, transmission lines

Abstract*: The current paper presents an artificial intelligence based technique applied in the investigation of electromagnetic interference problems between high voltage power lines (HVPL) and nearby underground metallic pipelines (MP). An artificial neural network (NN) solution has been implemented by the authors to evaluate the inductive coupling between HVPL and MP for different constructive geometries of an electromagnetic interference problem considering a multi-layer soil structure. Obtained results are compared to solutions provided by a finite element method (FEM) based analysis and considered as reference. The advantage of the proposed method yields in a simplified computation model compared to FEM, and implicitly a lower computational time.*

1. INTRODUCTION

Due to economic policies meat to reduce construction costs and European ecological regulations respectively, various utilities like gas, oil or water transportation pipelines have been forced to share for several kilometers the same distribution corridors as overhead high voltage power lines and/or AC railway systems.

The electromagnetic fields produced by high voltage transmission lines result in AC interference to nearby metallic structures. Therefore, in many situations gas, oil or water transportation metallic pipelines are exposed to the effects of induced AC current and

voltages that could be dangerous both on the operating personal and the pipeline structural integrity due to electrochemical corrosion [1-4].

Evaluation of induced currents and voltages in underground metallic pipelines placed in the vicinity of overhead power lines tend to be a complex issue, because many interrelations between them exist. To solve the differential equations which describe the electromagnetic field distribution and the existing coupling mechanism it assumes in most of the cases the use of specific numerical methods, like FEM, which transforms the electromagnetic interference problem into a numerical one [5].

Although FEM yielded solutions are very accurate, regarding to the problem complexity, the computing time of this method increases with the geometry, its mesh and required evaluation parameters. As a result the investigation of HVPL-MP electromagnetic interference problems for different system configurations requires expensive computing time because each new problem geometry involves a new mesh and a new FEM calculations. Therefore, any scaling method of the results from one configuration to another that requires less computing time, may be of interest.

A first attempt in applying artificial intelligence techniques to scale HVPL-MP interference results was made by Satsios et al. [6, 7]. A Fuzzy Logic Block (FLB) was implemented to evaluate the Magnetic Vector Potential (MVP) in case of a phases to ground fault on the HVPL. However, the implemented FLB provide relatively good results, the main disadvantage of this method consists in determination of the optimal parameters, which describes the fuzzy logic rule base. An iterative technique based on conjugate gradient method has been used [6]. Later on a Genetic Algorithm technique had been proposed by Damousis to determine the optimal rule base [8].

Another artificial intelligence approach has been presented by Al-Badi et al. [9, 10] applying a feed-forward Neural Network (NN) to evaluate the induced AC interferences in an underground pipeline in case of a similar phase to ground fault. The main advantage of this NN solution was that it provided directly the value of the induced AC voltages.

Based on the previous experience obtained implementing feed-forward [11] and layer recurrent [12] NN for the evaluation of the MVP in case of phase to ground faults, in the current work the authors have developed a feed forward NN that evaluates directly the HVPL-MP inductive coupling matrix elements. The proposed NN solution enables the evaluation of the induced AC currents and voltages in both HVPL normal operating and phase to ground fault condition, considering a vertically layered soil structure.

2. STUDIED ELECTROMAGNETIC INTERFERENCE PROBLEM

The electromagnetic interference problem between an underground gas transportation metallic pipeline and a nearby high voltage single circuit 220 kV / 50 Hz transmission line is investigated. The underground pipeline and the overhead power line share the same distribution corridor for a distance of 10 km. The induced A.C. currents and voltages in the metallic pipeline are analyzed in both HVPL normal operating and phase to ground fault conditions, when the fault appears far away outside the common right-of-way. For a more realistic problem representation a multilayer earth configuration, with three vertical soil layers is considered, as in *figure 1* can be seen:

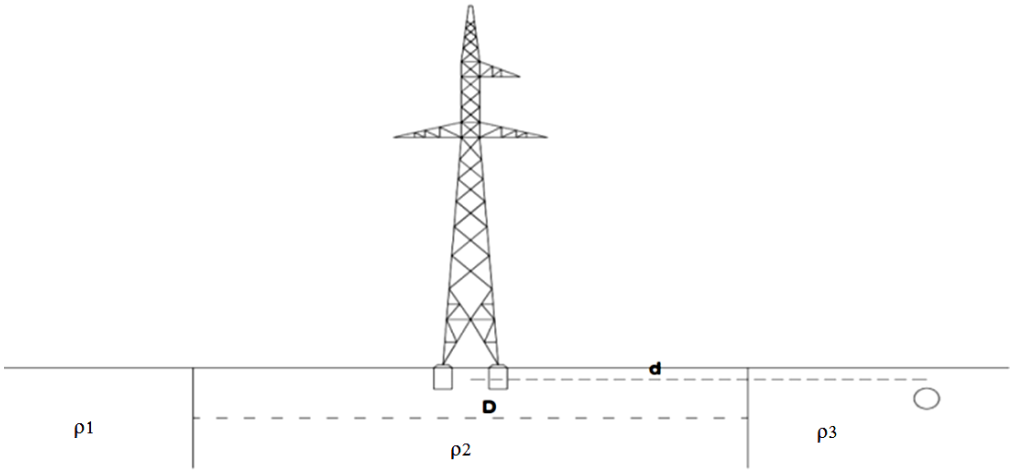

Fig. 1 – Cross section of the investigate electromagnetic interference problem

The underground gas pipeline consists in a steel alloy with a 5.882 MS/m bulk conductivity and a μ_r = 300 relative magnetic permeability. It has 22 cm outer radius a 8 mm thickness and 4.2 mm polyethylene insulation and it is buried at 1.5 m depth. The overhead power line consists in three phase wires and one ground wire placed in delta configuration on IT.Sn102 type metallic transmission line towers. *Table 1* presents the actual position of phase and ground wires on power line towers:

Table 1. Transposing principle

Conductor	Position [m]	Height [m]
Phase Wire A (0°)	2.85	21.4
Phase Wire B (-120°)	-5.3	17.2
Phase Wire C (-240°)	-3.2	17.2
Ground Wire	0	24.7

The electromagnet interference between on overhead transmission line and any nearby metallic structure could be as a results of the following coupling mechanisms [13, 14]:

- Inductive Coupling: Electromotive forces induced by the time varying magnetic field produced by transmission line A.C. currents causes current circulation an voltages between nearby metallic structures and surrounding earth.
- Conductive Coupling: When a ground fault occurs the current flowing through trough transmission line grounding grid produce a potential rise on both the grounding grid and the neighboring soil with regard to remote earth. If the metallic structure is close enough this potential rise could be transferred to it.
- Capacitive Coupling: Affects mostly above ground structures and occurs due to the capacitance between the power line and the nearby metallic structure. Due to earth's screening effect, the capacitive coupling may be neglected in case of underground structures.

Therefore, in our situation, taking into consideration that the phase to ground fault appears far away outside the common right-of-way, only the inductive coupling between the power line and the nearby underground pipeline has to be investigated. For this, first the electromagnetic field distribution around the transmission line has to be analyzed. Considering the cross-section of the common right-of-way the following system of equations describes the linear 2D electromagnetic diffusion problem for the z-direction components A_z of the magnetic vector potential and J_z of the total current density vector is obtained [15]:

$$\begin{cases} \dfrac{1}{\mu_0\mu_r}\cdot\left[\dfrac{\partial^2 A_z}{\partial x^2}+\dfrac{\partial^2 A_z}{\partial y^2}\right]-j\omega\sigma A_z+J_{sz}=0 \\ -j\omega\sigma A_z+J_{sz}=J_z \\ \iint\limits_{S_i} J_z\,ds=I_i \end{cases} \tag{1}$$

where J_{sz} is the source current density in the z direction and I_i is the imposed current on conductor i of S_i cross section.

Usually equation (1) is solved locally through finite element calculation. Using the values of the magnetic vector potentials, the self and mutual inductances can be calculated using the relations (2) and (3) [16, 17]. Considering a situation where only one of the conductors is energized and a null current is imposed on all the other conductors applying Faraday's Law the self-inductance of energized conductor and the mutual inductance component in all the other conductors due to the energization current can be evaluated based on the magnetic vector potential obtained on the cross-section of each conductor by solving equation (1):

$$L_{i,i}=\frac{\overline{A_{z\,i}}\cdot l}{\bar{I}_i} \tag{2}$$

$$L_{i,j}=\frac{\overline{A_{z\,j}}\cdot l}{\bar{I}_i} \tag{3}$$

where: $L_{i,i}$ and $L_{i,j}$ are conductor i self-inductance and the mutual inductance between conductor i and j respectively, A_{zi} and A_{zj} are the magnetic vector potential on the cross-section of conductor i and j due to energization current I_i and l is the length of the common right-of-way.

Applying a permutation of the energization current on each conductors, one can determine the self and mutual inductance matrix, which describes the inductive coupling between the power line and the nearby gas pipeline [18].

3. NEURAL NETWORK APPROACH

In order to do not rerun the finite element calculation each time a different problem geometry is investigated, the author have developed an artificial neural network that provides the inductive coupling matrix elements for any possible problem geometry. In comparison to previously proposed NN solutions the implemented feed-forward NN allows the evaluation of induced currents and voltages in the underground pipeline for both normal and far away phase to ground HVPL fault operating conditions.

A. The General Structure of an Artificial Neural Network

The concept of an artificial neural network has been inspired by the operation process of the human brain. The major building block of a neural network, the artificial neuron (see *figure* 2), like the biological one is a system with a variable number of inputs u_k, $k=\overline{1,m}$ and only one output.

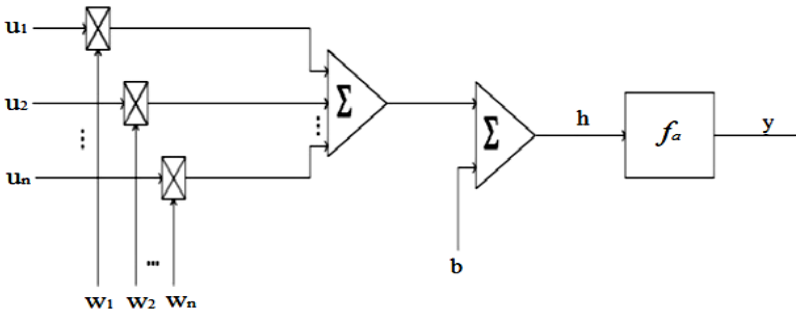

Fig. 2 – Structure of an artificial neuron

The weighted inputs sum is added to a parameter b called bias [18] and provided as argument to a transfer function, which evaluates the output value of the artificial neuron. The transfer function, equation (4), is specific to each neuron and is the equivalent to the nucleus of a biological neuron:

$$y = f_a(h) \text{ where } h = \sum_{k=1}^{m}(u_k \cdot w_k) + b \tag{4}$$

A group of artificial neuron that work in parallel, have the same inputs and the outputs have the same destination form a layer. Multiple interconnected neuron layers form the structure of an artificial neural network. The neurons that provide the output values of the NN form the output layer, whereas all the other neuron layers are called hidden layers. The architecture of neural network is specific to the application for which is implemented. Unusually in electrical engineering applications the classical feed-forward architecture is used (see *figure 3*) [19]:

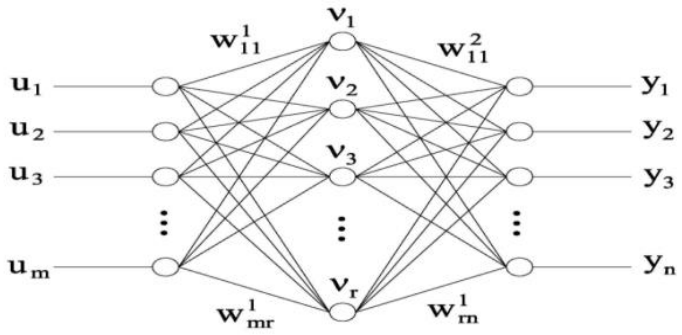

Fig. 3 –Feed-forward neural network with one hidden layer

From the above architecture the equations defining output values of a feed-forward neural network can be developed if the inputs are knowns. The hidden layer neurons output is driven by the following relation:

$$v_j = f_{a1}\left(h_j^1\right) = f_{a1}\left(\sum_k \left(u_k \cdot w_{kj}\right) + b_j^1\right) \tag{5}$$

Therefore, the final outputs of a feed-forward neural network will be given by [19]:

$$y_i = f_{a2}\left(h_i^2\right) = f_{a2}\left(\sum_j \left(w_{kj} \cdot f_{a1}\left(h_j^1\right)\right) + b_j^2\right) \tag{6}$$

In order to provide the desired output values an artificial neural network has to be trained. During the training process the weights and biases of each neuron from the network are continuously adjusted through a back propagation algorithm in accordance to the error between the actual NN output and the desired values. This error is evaluated by a performance function. In most of the cases the mean square error, equation (7), is used as performance function [19]:

$$Err = \frac{1}{n} \cdot \left(\sum_{i=1}^{n} \left(y_i^* - y_i\right)^2\right) \tag{7}$$

B. Proposed Neural Network Implementation

To implement the proposed neural network approach MATLAB's Neural Network toolbox has been used. Based on the previous experience obtained implementing feed-forward [11] and layer recurrent [12] NN for the evaluation of the MVP in case of phase to ground faults, the authors have decided to develop a feed-forward architecture. The input parameters of the proposed NN has been set to:

- d – separation distance between HVPL and MP (which varies between 0 m and 1000 m);
- ρ_1, ρ_2, ρ_3 – resistivity of the left side, middle and right side soil layer respectively (which varies between 10 Ω·m and 5000 Ω·m);
- D – earth middle layer width (which varies between 20 m and 1200 m);

During the pre-processing stage of proposed NN solution all the input parameters are automatically scaled by MATLAB to the [-1,+1] range. The output values are the inductance matrix elements which describe the HVPL-MP inductive couplings. Taking into account that the inductance matrix is a symmetrical one, only the elements above the main diagonal have been considered. Therefore, for the investigated HVPL-MP electromagnetic interference problem (3 phase wires, 1 ground wire and one pipeline) the provided matrix elements will be: $L_{11}, L_{12}, L_{13}, L_{14}, L_{15}, L_{22}, L_{23}, L_{24}, L_{25}, L_{33}, L_{34}, L_{35}, L_{44}, L_{45}, L_{55}$, where L_{ii} representing the self-inductance of conductor i and L_{ij} the mutual inductance between conductor i and j respectively (with for phase wires, i=4 for the ground wire and i=5 for the pipeline).

After analyzing in detail the inductance matrix values obtained through FEM calculation for different problem geometries the authors concluded that in order to increase accuracy and reduce training time to implement three different neural networks: NN1 to evaluate conductors self-inductance $(L_{11}, L_{22}, L_{33}, L44, L55)$, NN2 for the mutual inductances involving the pipeline $(L_{15}, L_{25}, L_{35}, L_{45})$ and NN3 all the other mutual inductance elements.

To train the implemented NN architectures a training data base has been used containing inductive coupling matrix elements obtained through FEM analysis of different

HVPL-MP problem geometries. To obtain a useful training database approximately 4500 different problem geometries have been investigated varying the HVPL-MP separation distance from 0 m to 1000 m, the soil resistivity values from 10 Ω·m to 5000 Ω·m and the middle layer width from 20 m to 1500 m. Table 2 presents some of the problem geometries used to train the implemented neural networks.

Table 2. Training HVPL-MP problem configurations

Case No.	d [m]	D [m]	ρ_1 [Ω*m]	ρ_2 [Ω*m]	ρ_3 [Ω*m]	Case No.	d [m]	D [m]	ρ_1 [Ω*m]	ρ_2 [Ω*m]	ρ_3 [Ω*m]
8	5	60	500	50	500	2134	0	550	50	250	50
104	100	60	150	250	150	2301	20	550	30	250	30
206	20	60	50	500	50	2532	100	550	100	500	100
373	100	60	500	750	500	2751	500	550	30	100	30
481	150	60	500	250	500	2914	5	1050	10	250	10
692	1000	60	750	50	750	3096	20	1050	100	250	100
875	20	120	100	750	100	3274	100	1050	500	1000	500
1064	50	120	750	1000	750	3545	750	1050	30	750	30
1231	500	120	100	30	100	3754	5	1500	50	30	50
1391	0	240	50	10	50	3969	35	1500	10	250	10

1505	0	240	1000	750	1000	4106	750	1500	50	10	50
1891	250	240	500	30	500	4320	1000	1500	250	1000	250
2022	500	240	750	50	750	4442	750	240	50	50	50

In order to identify the optimal solution for each of the proposed neural networks, different feed-forward architectures with one output layer and two hidden layers were implemented (see *figure* 4). The number of neuros in each hidden layer was varied from 5 to 30, the transfer function of the hidden layers were set consecutively to *tansig* (hyperbolic tangent sigmoid function, equation (8)), logsig (logarithmic sigmoid function, equation (9)) and purelin (linear function) whereas the transfer function of the output layer neurons has been set to purelin.

$$f(h)=\frac{1-e^{-2h}}{1+e^{-2h}} \tag{8}$$

$$f(h)=\frac{1}{1+e^{-h}} \tag{8}$$

The performance evaluation function was set to mse (mean square error, equation (7)) and the descendent gradient with momentum weight learning rule was selected to train the neural networks using the Levenberg-Marquardt method.

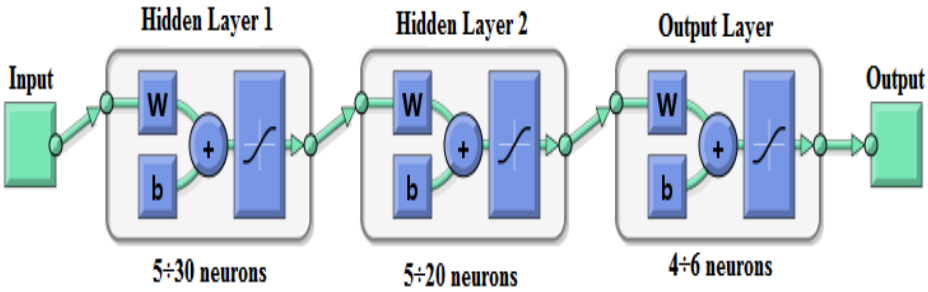

Fig. 4 – Implemented feed-forward network architecture

3. NEURAL NETWORK RESULTS

The training process took between 1 and 10 minutes on a i7-3632QM 2.2GHz Intel Core PC, with a 64 bit operating system and 8 GB RAM memory. Once the implemented neural network architectures were trained, to identify the optimal NN solution, the error between the output values provided by each NN and the finite element results, considered as reference, were evaluated.

Table 3. Testing HVPL-MP problem configuration

Case No.	d [m]	D [m]	ρ_1 [Ω*m]	ρ_2 [Ω*m]	ρ_3 [Ω*m]	Case No.	d [m]	D [m]	ρ_1 [Ω*m]	ρ_2 [Ω*m]	ρ_3 [Ω*m]
1	310	800	900	850	900	15	310	800	900	850	900

3	105	1100	550	550	550	17	170	700	300	350	300
5	250	800	150	150	150	19	240	500	80	750	80
7	340	400	600	150	600	21	420	100	550	20	550
9	170	800	650	750	650	23	105	1200	250	950	250
10	55	1000	900	400	900	25	85	400	140	160	140
11	40	200	600	800	600	28	15	300	140	700	140
13	120	900	750	350	750	30	10	1000	200	750	200

In order to determine the accuracy of the implemented NN architectures in case of new HVPL-MP electromagnetic interference problem configurations, in the NN testing procedure not only the training data base was used, but also a second data set that was not applied during the training process. *Table 3* presents the randomly generated HVPL-MP problem geometries used to test the implemented NN architectures

In case of the neural network used to evaluate the self-inductance of each conductor from the investigate HVPL-MP interference problem, the optimal NN1 architecture is a feed-forward NN with two hidden layers using the *tansig* transfer function: 15 neurons on the first layer and 25 neurons on the second hidden layer. The average evaluation error is 0.043% for the training data base and 0.064% for the testing data set, respectively. The maximum obtained evaluation errors were 0.77% and 0.20% respectively. *Figure 5* presents the error distribution for the training and testing problem geometry data sets:

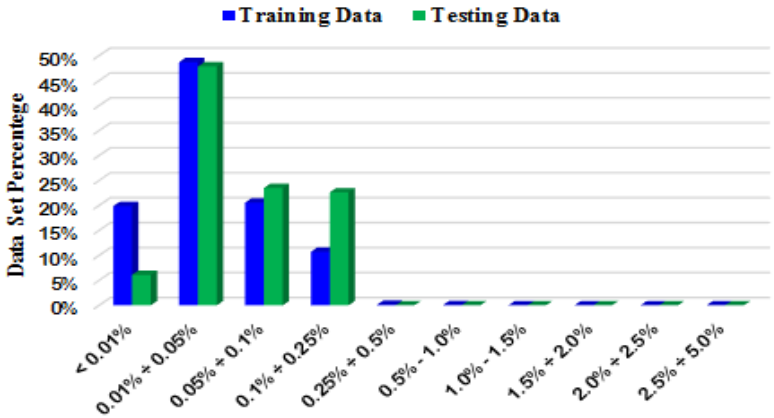

Fig. 5 – Evaluation error distribution for the optimal NN1 architecture

For the neural network implemented to evaluate the mutual inductance values between the underground pipeline and all the other conductors, the optimal NN2 architecture is a feed-forward NN using the *logsig* transfer function and having 30 neurons on the first hidden layer and 25 neurons on the second one. This NN configuration provided an average 0.058% and 0.052% evaluation error for the training data base and the testing data set respectively, whereas the maximum obtained evaluation errors were 2.67% and 0.14% respectively. *Figure 6* presents the error distribution for the training and testing problem geometry data sets:

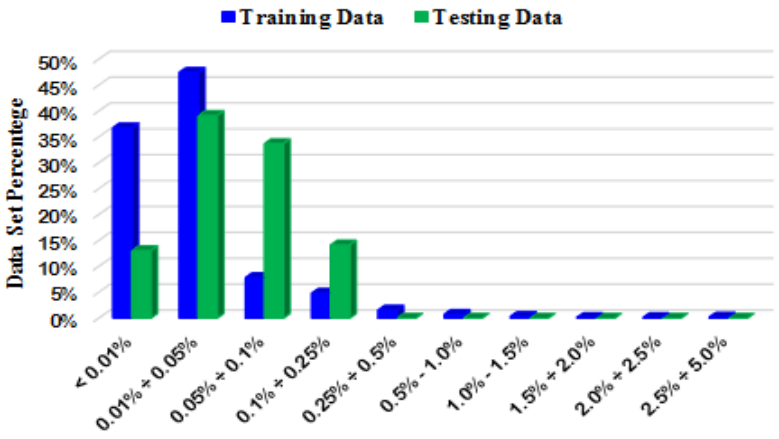

Fig. 6 – Evaluation error distribution for the optimal NN2 architecture

In case of the neural network used to evaluate the mutual inductance values between the HVPL phase and ground wires, the identified NN3 optimal architecture with two hidden layer feed-forward NN with 25, respectively 15 neurons on its hidden layers and using a tansig transfer function. The evaluation error for this optimal NN3 configuration presents and average value of 0.029% and 0.020% for the training and respectively testing data sets, whereas the maximum evaluation error values are 2.56% and 0.069% respectively. Fig. 7 presents the error distribution for the training and testing problem geometry data sets.

Combining the results provided by the above presented three optimal NN configuration the inductive coupling matrix values can be determined for any HVPL-MP problem geometry, with an average 0.1% evaluation error (not exceeding 3% in any case).

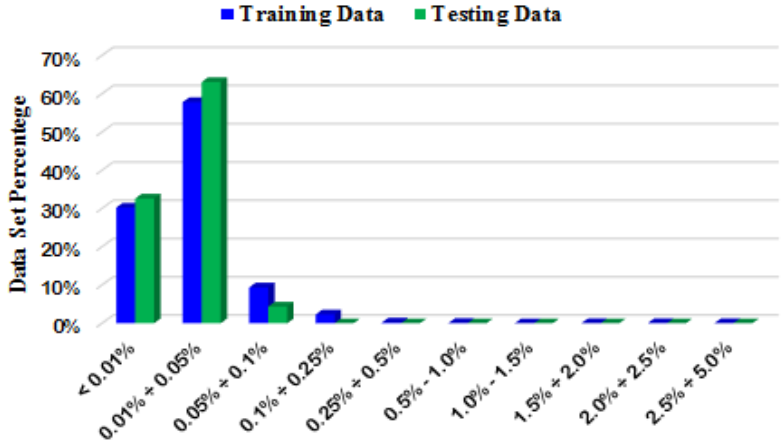

Fig. 7 – Evaluation error distribution for the optimal NN3 architecture

Table 4 presents the obtained self and mutual inductance values describing the inductive coupling between HVPL and the nearby underground pipeline in case of a 30 m separation distance and vertically layers soil structure with ρ_1 = 500 Ω·m, ρ_2 = 30 Ω·m and ρ_3 = 500 Ω·m, considering a 20 m width for the middle layer:

Table 4. Testing HVPL-MP problem configuration

Self and Mutual Inductances [μH/m]					
	PhW A	**PhW B**	**PhW C**	**GrndW**	**Pipe**
PhW A	2.45	1.234	1.110	1.187	0.82
PhW B	1.234	2.45	1.100	1.073	0.84
PhW C	1.110	1.100	2.45	1.073	0.80
GrndW	1.187	1.073	1.073	8.74	0.79
Pipe	0.822	0.842	0.80	0.795	2.28

4. INDUCED CURRENTS AND VOLTAGES

Based on the self and mutual inductance values provided by the proposed neural network solution the equivalent electrical circuit of the investigated HVPL-MP electromagnetic interference problem can be constructed (see *figure 8*). Applying a one side unknown elimination solver based on loop currents method, like the one implemented in the *InterfStud* software application developed by the authors in a previous work [20], the induced A.C. currents and voltages in the metallic pipeline can be evaluated.

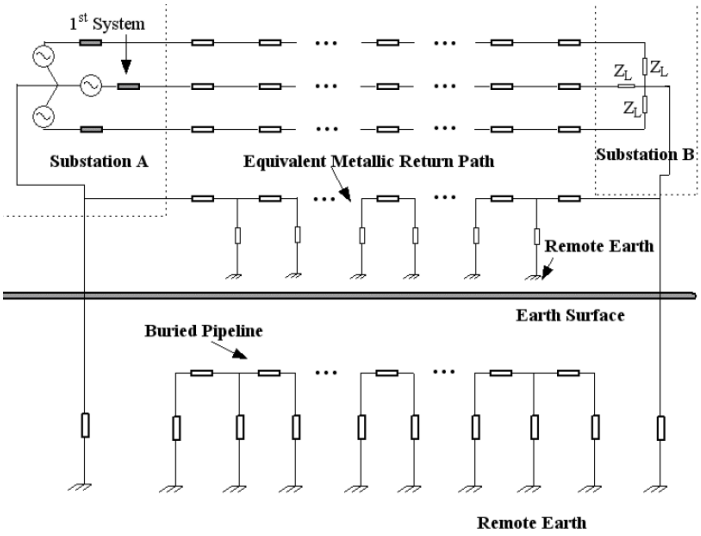

Fig. 8 – HVPL-MP equivalent electrical circuit

A. Steady State HVPL operating conditions

Providing the self and mutual inductance matrix, obtained as output data from the implemented NN solution, to the InterfStud software application the induced current and voltage values have been evaluated considering a steady state HVPL operating condition with a 350 A symmetrical current load on power line phase wires (130 MVA three phase load with a 0.94 power factor). Three different problem geometries have been analyzed:

- ***Geometry 01***. A 30 m HVPL-MP separation distance, considering the following soil structure: $\rho_1 = \rho_3 = 500\ \Omega\cdot m$, $\rho_2 = 30\ \Omega\cdot m$, with a 20 m width middle layer;

- ***Geometry 02.*** A 50 m HVPL-MP separation distance, considering the following soil structure: $\rho_1 = 10\ \Omega\cdot m$, $\rho_2 = 100\ \Omega\cdot m$, $\rho_3 = 500\ \Omega\cdot m$ with a 30 m width middle layer;
- ***Geometry 03.*** A 150 m HVPL-MP separation distance, considering the following soil structure: $\rho_1 = \rho_2 = 100\ \Omega\cdot m$, $\rho_3 = 1000\ \Omega\cdot m$, with a 100 m width middle layer;

Figure 9 presents the obtained induced current values along pipeline line length, whereas *figure 10* presents the evaluated induced voltage values. Due the fact that the gas pipeline is electrically insulated at the common right-of-way ends from the rest of the stream gas network the maximum induced voltage level are obtained at right-of-way ends, whereas the induced current reaches its maximum value at right-of-way midsection.

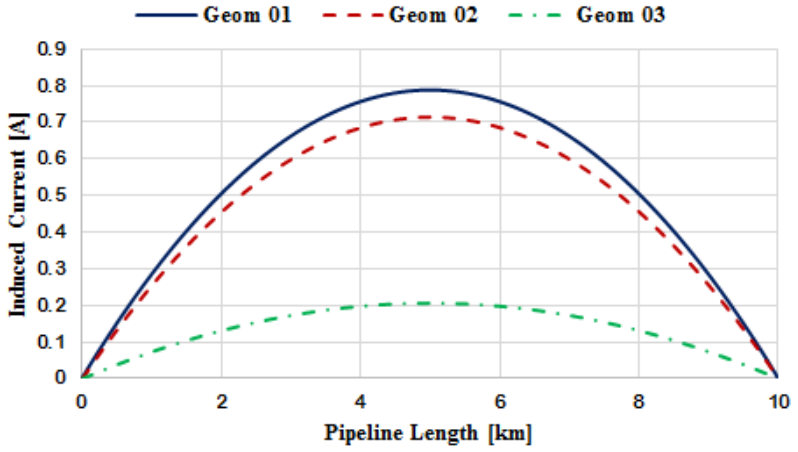

Fig. 9 – Induced current in the underground metallic pipeline for different HVPL-MP problem geometries

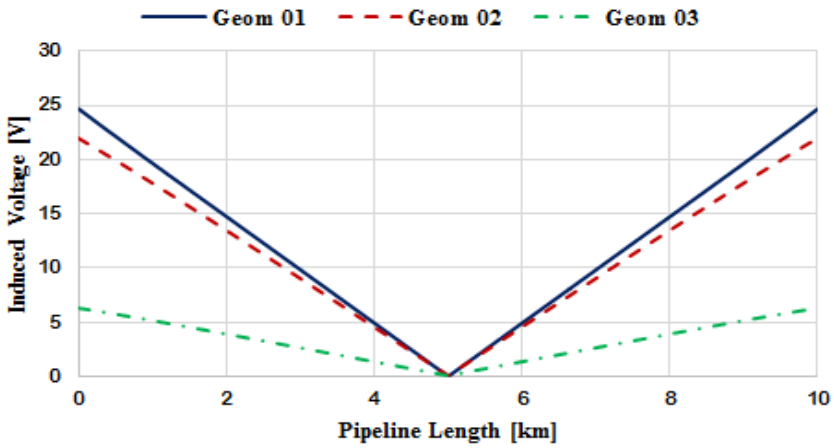

Fig. 10 – Induced voltage in the underground metallic pipeline for different HVPL-MP problem geometries

B. Phase to ground fault HVPL operating conditions

Finally the induced A.C. current and voltages in the underground gas pipeline are evaluated in case of a phase to ground HVPL fault that appears far away outside the common distribution corridor. It is considered that 1500 A current flows through the faulted phase wire

(phase A), whereas the same steady state load current flows through the other two healthy phase wires (phase B and C). *Figure 11* presents the obtained induced voltage values along pipeline length for the three investigated problem geometries. It can be observed that the induced voltage values decrease with the separation distance, however an increase is recorded if the soil resistivity in the near proximity of HVPL-MP right-of-way is increased (see *figure 10* and *figure 11*).

5. CONCLUSION

A neural network based artificial intelligence technique has been implemented by the authors to scale from a known set of problem geometries the inductive coupling matrix for any possible geometrical configuration of a HVPL-MP electromagnetic interference. The proposed neural network approach reduces considerably the computation time of the self and mutual inductance values that describe the inductive coupling between the HVPL and the nearby MP.

From *figure 5÷7* it can be observed that the evaluation error produced by the identified optimal NN architecture are usually less than 0.1% in comparison to the finite element results considered as reference. Therefore, the implemented neural network solution to evaluate the self and mutual inductance values is a very effective one, especially if we take into account the fact that the solutions provided by neural networks are obtained almost instantaneously and can be used to evaluate the induced currents and voltages in both HVPL normal and phase to ground fault operating conditions.

ACKNOWLEDGEMENT

This work was supported by the Post-Doctoral Programme POSDRU 159/1.5/S/137516, project co-funded from European Social Fund, through the Human Resources Sectorial Operational Program 2007-2013.

REFERENCES

[1]. CIGRE, *Guide concerning influence of high voltage AC power systems on metallic pipelines*, CIGRE Working Group 36.02, Canada, 1995.

[2]. EN 50443, *Effects of electromagnetic interference on pipelines caused by high voltage A.C. railway systems and/or high voltage A.C. power supply systems*, CENELEC, European Committee for Electrotechnical Standardization, ICS 33.040.20; 33.100.01, January, 2009.

[3]. R. Baboian, *NACE Corrosion Engineer's Reference Book*, NACE International, Huston, USA, 2002.

[4]. R. Zhang, P. R. Vairavanathan, S. B. Lalvani, *Perturbation method analysis of AC-induced corrosion*, Corrosion Science, vol. 50, pp. 1664-1671, 2008.

[5]. D.D. Micu, I. Lingvay, C. Lingvay, L. Darabant, A. Ceclan, *Numerical evaluation of induced voltages in the metallic underground pipelines*, Revue Roumaine des Sciences Techniques Serie Électrotechnique et Énergetique, vol. 54, no. 2, pp. 175-184, 2009.

[6]. K. J. Satsios, D. P. Labridis, P. S. Dokopoulos, *An Artificial Intelligence system for a complex electromagnetic field problem: Part I – Finite element calculations and Fuzzy Logic development*, IEEE Trans. on Magnetics, vol. 35, no. 1, pp. 516-522, 1999.

[7]. K.J. Satsios, D.P. Labridis, P.S. Dokopoulos, *An Artificial Intelligence system for a complex electromagnetic field problem: Part II – Method implementation and performance analysis*, IEEE Trans. on Magnetics, vol. 35, no. 1, pp. 523-527, 1999.

[8]. I.G. Damousis, K.J. Satsios, D.P. Labridis, P.S. Dokopoulos, *Combiend Fuzzy Logic and Genetic Algorithm techniques – Application to an electromagnetic field problem*, Fuzzy Sets and Systems, vol. 129, no. 3, pp. 371-386, 2002.

[9]. A. Al-Badi, K. Ellithy, S. Al-Alawi, *An Artificial Neural Network model for predicting gas pipeline induced voltage caused by power lines under fault conditions*, COMPEL: The International Journal for Computation and Mathematics in Electrical and Electronic Engineering, vol. 24, no. 1, pp. 69-80, 2005.

[10]. A. Al-Badi, K. Ellithy, S. Al-Alawi, *Prediction of voltage on mitigated pipelines paralleling electric transmission lines using an Artificial Neural Network*, The Journal of Corrosion Science and Engineering, vol. 10, Preprint 28, 2007.

[11]. D.D. Micu, L. Czumbil, G.C. Christoforidis, E. Simion, *Neural Networks applied in electromagnetic interference problems*, Revue Roumain des Sciences Techniques, Serie Électrotechnique et Énergetique, vol. 57, no. 2, pp. 162-171, 2012.

[12]. D.D. Micu, L. Czumbil, G.C. Christoforidis, A. Ceclan, *Layer recurrent Neural Network solution for an electromagnetic interference problem*, IEEE Trans. on Magnetics, vol. 47, no. 5, pp. 1410-1413, May, 2011.

[13]. J. Ma, F. P. Dawalibi, *Recent advances in electromagnetic analysis in common corridors*, in Proceedings of the 4th Asia-Pacific Conference on Environmental Electromagnetic (CEEM), pp. 409-418, Dalian, China, 1-4 August, 2006.

[14]. D.D. Micu, A. Ceclan, L. Darabant, D. Stet, *Analytical and numerical development of the*

electromagnetic interference between a high-voltage power line and a metallic underground pipeline, in Proceedings of the 8th International Symposium on Advanced Electromechanical Motion Systems & Electric Drives Joint Symposium, Lille, France, 1-3 July, 2009.

[15]. G.C. Christoforidis, D.P. Labridis, P.S. Dokopoulos, *Inductive interference calculation on imperfect coated pipelines due to nearby faulted parallel transmission lines*, Electric Power Systems Research, vol. 66, no. 2, pp. 139-148, August, 2003.

[16]. G.C. Christoforidis, D.P. Labridis, *A hybrid method for calculating the inductive interference caused by faulted power lines to nearby buried pipelines*, IEEE Trans. on Power Delivery, vol. 20, no. 2, pp. 1465-1473, April 2005.

[17]. L. Czumbil, D. Stet, D.D. Micu, V. Ţopa. L. Ancas, *Stream gas pipeline in proximity of high voltage power lines. Part II - Induced voltage evaluation*, in Proceedings 47th Internatonal Universities' Conference on Power Energy (UPEC), London, UK, 4-7 September, 2012.

[18]. M. Caudil, C. Butler, *Understanding Neural Networks: Computer Exploration*, vol. 1 and vol. 2, MA: the MIT Press, Cambridge, U.K., 1992.

[19]. S. Razavi, B.A. Tolson, *A new formulation for feedforward Neural Networks*, IEEE Trans. on Neural Networks, vol. 22, no. 10, pp. 1588-1598, 2011.

[20]. L. Czumbil, G.C. Christoforidis, D.D. Micu, D. Stet, A. Ceclan, O. Pop, *A user-friendly software application for induced A.C. interference evaluation*, in Proceedings of the 46th International Universities' Power Engineering Conference (UPEC), Soest, Germany, 5-8 September, 2011.

A SYSTEM FOR REMOTE MONITORING OF THE HUMAN BODY PARAMETERS

Oliviu **MATEI**[1], Claudia **MATEI**[2], Ioan **VLAD**[3], Cristinel **COSTEA**[1]
[1] *Technical University of Cluj-Napoca,North University Centre of Baia Mare,*
[2] *Active Aging Association,* [3] *Intellisoft Association*
oliviu.matei@cunbm.utcluj.ro, cabdia@yahoo.com, ioan.vlad@intellisoft.ro,
cristinel.costea@cunbm.utcluj.ro

Keywords: Genetic algorithms, Wearable computers.

Abstract*: We present an invention (pending patent number A 201100939) related to a system that monitors human body parameters, such as heart rate and blood pressure, and when they are out of the regular range, it transmits a remote warning signal along with the GPS coordinates of the patient to the special intervention services, or to the tutors, so that they can take action in the shortest time. The most important aspect of the system is its mobility, the patient being able to live her normal life, not having to stay in a fix perimeter, as it is the case for most monitoring equipments. The scope of the invention is the health of people, both individually and at the institutions involved in health insurance, such as clinics, hospitals, emergency services, rescue, SMURD, social settlements, etc.*

1. INTRODUCTION

A majority of older adults are challenged by chronic and acute illnesses and/or injuries. Hence, chronic disease management, post-acute care management, and safety monitoring are three important applications of remote patient monitoring (RPM) technologies for the older adult population, and not only. RPM technologies can help monitor the patients after surgical interventions or in case of chronic diseases. RPM technologies can also alert care givers and prompt intervention when a vulnerable older adult is injured or in harms way.

More than 70% of the strokes in the case of elders generate significant variations in heart rate or pulse, therefore it is important to monitor these human body parameters in order to prevent or to intervene in a critical period of time.

A. Related work

Worldwide, many other systems that monitor different parameters of human body are known, especially hospitals or other health institutions. Also, other ”home usage systems” are known, systems being in the reach of the patient, mostly outside the health institutions, systems that monitor different parameters of human body, especially blood pressure, the recorded value being revealed to the patient either by a traditional display or by a digital one. the disadvantage of this system is that patients should know the normal range of blood pressure values, to determine whether the recorded value is within the normal range or not.

Several systems for monitoring biological signals use radio waves and telephone lines. The disadvantages of these solutions are generated by their low performance, their complexity, allowing identification of the subject and the occurrence of an emergency situation, this information being sent to a third person rather to the one in question.

For example the monitoring and warning system related to vital physiological parameters of persons exposed to risk factors because their work is carried out under extreme conditions (in depth or height, in narrow spaces, extreme temperatures, thin or flawed atmosphere, etc.) [5] has the main disadvantages of requiring a multitude of devices: monitoring equipment, and some portable interfaces, including a tactical technique, all occupying a relatively large space and are operated by someone other than those monitored. also, another disadvantage is that this system addresses only to a certain category of people, not to everyone.

The system for monitoring biological signals presented by the patent [6] has the major disadvantage is that, although it can monitor a large number of subjects, it is only intended for medical offices, which are served by staff who have the human biological parameters.

The patent [7] refers to a detector of vital body functions in order to monitor pulse, blood pressure, etc. and transmission of measured values for display and storage on a daily communication terminal comprising a sensory way, communications equipment and an external GPS system. The disadvantages of this solution are: because of how it is designed, the system works continuously, transmits values continuously and thus consumes significant energy, and periodic maintenance of the system is required, also causing rapid wear of the component equipment.

2. ARCHITECTURE OF THE SYSTEM

The system comprises of two major parts (see figure 1): a sensory module (8) and a communication equipment (1), e.g. a smart phone.

The sensory module is composed of sensors (9) for pulse, heart rate, temperature etc., which sends the signal to an amplifier (10), which, in turn, sends the signal to a microcontroller (11). This is responsible for processing the information and decide whether there are significant variations of the signal, which are to be sent to the communication equipment. If there are significant variations, the data is transferred through a communication interface (12). Due to the microcontroller, the communications between the two modules, (8) and (1) are minimal, which leads to important energy savings.

The data sent by the sensory module (8) is received by the equipment (1) through a communication interface (2), similar to the interface (12). Then they are send further to the processor (6), which uses some complex algorithms for deciding if the values sensed by the sensor (9) are in normal ranges. If not, a message is shown on the display (7). Moreover, the information along with the geo-spatial coordinates collected by the GPS (5) are sent as vocal or written message (e.g. SMS, MMS) and over the Internet (as an email or by connecting to a server, through a client-server application).

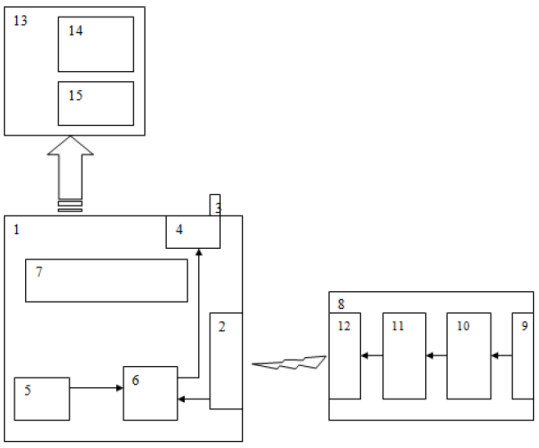

Fig. 1 - The architecture of the system

The application (13) shows on a map (14) the location of the surveyed person and by means of a special software module draws the optimal routes to her.

The sensory module (8) is like a bracelet or more like a wrist watch and contains the sensor (9), the operational amplifier (10), the microcontroller (11) and the communication interface (12). The sensors can be multiple, e.g. for pulse, heart rate, temperature etc. The most needed and useful ones are the for pulse and heart rate. The amplifier (10) is needed to

increase the signal from the sensor (9) and send it to the microcontroller (11). The microcontroller can read the values and compare them with the regular ones, for each type of sensor. It is very important because it reduces the communication between module (8) and (1) significantly. As the data is read every 5 seconds, a (wireless) connection between the two modules would be established every 5 seconds. Such a connection requires much energy, that is why the microcontroller sends alerts to the communication module (1) only when needed.

The communication terminal (1) may be a smart phone, but not necessarily. It contains a (wireless) communication interface (2) similar with the interface (12) and may be a bluetooth module. The processor (6) controls the entire device (1) and receives data from the GPS (5). For any smartphone, the GPS (5) is embedded by default. The display (7) is used for the interface with the user. Module (4) is a GSM interface.

A. Activity diagram of the system

In order to make the worflow of the system explicit, we depicted in figure 2 the activity diagram. In the activity diagram shown in figure 2, the shapes represent:

- rectangles represent activities;
- rounded rectangles represent composed activities;
- bars represent the start (split) or end (join) of concurrent activities;
- diamonds represent decisions;
- an oval represents the start (initial state), respectively the stop (final state) of the workflow.

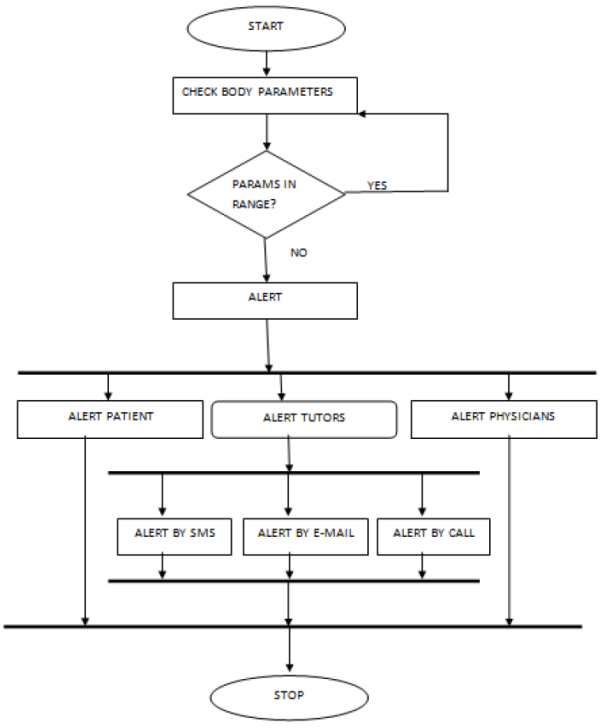

Fig. 2 - The activity diagram of the system

Arrows run from the start towards the end and represent the order in which activities happen. Hence they can be regarded as a form of flowchart. Typical flowchart techniques lack constructs for expressing concurrency. However, the join and split symbols in activity diagrams only resolve this for simple cases; the meaning of the model is not clear when they are arbitrarily combined with decisions or loops.

The diagram shows that the system never stops monitoring the body parameters (such as pulse and heart rate). If the values are out of normal ranges, an alert along with the GPS coordinates are emitted towards:

- the patient herself (on the display or by audio signal);
- the tutors, by e-mail, SMS or call;
- the supervising physicians (e.g. emergency room or ambulance service).

B. The sequence diagram of the system

To illustrate better the usage of the system, figure 3 depicts the sequence diagram. The processes and message involved among the modules are very simple, yet must be very robust because they are about the health of a human being.

As a matter of fact, between the two main modules there are only two types of messages: for initial pairing and when there are alerts regarding the values read by the sensor. We want to emphasize that the communication between the two modules is reduced as much as possible in order to save energy and the whole system must be very robust and it was designed having this in mind.

3. THE SERVER SIDE

The server-side software component is able to display the coordinates of the monitored patient on a map and route an ambulance to there. For a significant number of surveyed patients, the application is able to each medical team to more patients, if needed. That is done using an algorithm similar to the one presented by Pop and Matei in [9]. They describe a genetic algorithm for solving the generalized traveling salesman problem (GTSP). This problem is a generalization of finding a minimum cost Hamiltonian circuit or cycle of a given graph by considering instead of nodes node sets (clusters) and asking for finding a minimum cost Hamiltonian circuit or cycle which includes exactly one node from each cluster. This problem is called the generalized traveling salesman problem (GTSP) and it was introduced independently by Henry-Labordere [2], Srivastava et al. [14] and Saskena [12].

Further on we will present the algorithm.

A. Genetic Representation

An individual is represented as a pair (C, N), where $C = (V_1, V_2, \ldots, V_m)$ represents the sequence of clusters, described as Hamiltonian cycles. $N = (N_1, N_2, \ldots, N_m)$ represents the set of nodes selected from each cluster, meaning that the node N_k is the node selected from the cluster V_k. The individual $\mathrm{I} = (\mathrm{C}, \mathrm{N})$, with $C = (1, 5, 3, 4, 2)$ and $\mathrm{N} = (10, 23, 31, 44, 52)$ represents the tour which passes the clusters in the following order:

1-5-3-4-2-1

and the nodes as follows:

10-52-31-44-23-10

B. Initial population

The construction of the initial population is of great importance to the performance of GA, since it contains most of the material the final best solution is made of.

In our algorithm the initial population is generated separately for the set of clusters, respectively for the set of nodes selected from the clusters. Each cluster V_k is generated randomly from the set of the m m clusters. The set of nodes N_1 selected from the clusters is generated based on the Monte Carlo method. The first element N_1 is chosen randomly from the set of the nodes belonging to the cluster V_1. Each further node N_k, with $k \in \{2, \ldots, m\}$, is selected randomly inverse proportionally with the distance (cost) from its predecessor node: $d_k = c(N_{k-1}, N_k)$. The probability for each node to be selected is

$$p_i = \frac{d(N_i, N_k)}{D}, \text{ where } D = \sum_{k=1}^{|V_i|} d_k \tag{1}$$

It is obvious that the probability for a node to be chosen increased as the distance to the node N_k decreases. We define a summing probability:

$$D = \sum_{i=1}^{|V_i|} p_i \tag{2}$$

A random number $r \in [0,1]$ is chosen, which gives the node to be selected as being i which holds $r \in [q_i, q_{i+1})$.

Based on computational experiments we observed that this method assures an initial population with a fitness with 20% better than a population generated entirely randomly.

C. The fitness value

Every solution has a fitness value assigned to it, which measures its quality. In our case the, the fitness value of a feasible solution (generalized Hamiltonian tour) of the GTSP is given by

the total cost of the edges selected in the Hamiltonian tour i.e. the objective function of the integer programming model presented in the previous section. The aim is to find the generalized Hamiltonian tour with minimum cost.

D. Genetic operators

1) Crossover: Two parents are selected from the population by the binary tournament method, i.e. the individuals are chosen from the population at random.

Offspring are produced from two parent solutions using the following crossover procedure described by Matei in [3]: it creates offspring which preserve the order and position of symbols in a subsequence of one parent while preserving the relative order of the remaining symbols from the other parent. It is implemented by selecting a random cut point. The crossover operator for the set of nodes N is straightforward.

The recombination for the route C require some further explanations. First, the symbols before the cut points copied from the first parent into the offspring. Then, starting just after the cut-point, the symbols are copied from the second parent into the offspring, omitting any symbols that were copied from the first parent. The second offspring is produced by swapping round the parents and then using the same procedure.

Next we present the application of the proposed crossover for the cluster route C. We assume two well-structured parents chosen randomly, with the cutting point between 2 and 3:

$$C_1 = 1 \quad 4 \quad | \quad 2 \quad 3 \quad 5$$
$$C_2 = 2 \quad 1 \quad | \quad 5 \quad 4 \quad 3$$

The sequences before the cutting-point is copied into the two offspring:

$$O_1 = 1 \quad 4 \quad | \quad x \quad x \quad x$$
$$O_2 = 2 \quad 1 \quad | \quad x \quad x \quad x$$

The nodes of the parent C_1 are copied into the offspring O_2 if O_2 does not contain clusters in the as the nodes of C_1. Note the the cluster 2 is already represented in O_2. And the same holds for O_1 and C_2:

$$O_1 = 1 \quad 4 \quad | \quad 5 \quad x \quad 3$$
$$O_2 = 2 \quad 1 \quad | \quad x \quad 3 \quad 5$$

The already existing clusters are replaced by their correspondents from the other parent:

$$O_1 = 1 \quad 4 \quad | \quad 5 \quad 2 \quad 3$$
$$O_2 = 2 \quad 1 \quad | \quad 4 \quad 3 \quad 5$$

2)Mutation: We use in our GA two random mutation operators: the first one (intra-route mutation) selects randomly a cluster to be modified and replaces its current node by another one randomly selected from the same cluster and the second one (inter-route mutation) is a

swap operator, it picks two random locations in the solution vector and swaps their values. Similar mutation operators are reported by Pop et al. in [8].

The developed GA uses the steady-state approach, in which eligible offspring enter the population as soon as they are produced, with inferior individuals being removed at the same time, so that the size of the population remains constant.

3) Selection: The selection process is deterministic. The first selection is $(\mu+\lambda)$, where μ parents produce λ offspring. The new population of $(\mu+\lambda)$ is reduced again to μ individuals by a selection based of the "survival of the fittest" principle. In other words, parents survive until they are suppressed by better offspring. It might be possible for very well adapted individuals to survive forever. This feature yields some deficiencies of the method [1]:

1) In problems with optimum moving over time, a $(\mu+\lambda)$ selection may get stuck at an outdated good location if the internal parameter setting becomes unsuitable to jump to the new field of possible improvements.
2) The same happens if the measurement of the fitness or the adjustment of the object variables are subject to noise, e.g. in experimental settings.

In order to avoid effects, Schwefel investigated the properties of $(\mu+\lambda)$, selection, where μ parent produce $\lambda(\lambda>\mu)$ and only the offspring undergo selection. In other words, the lifetime of every individual is limited to only one generation.

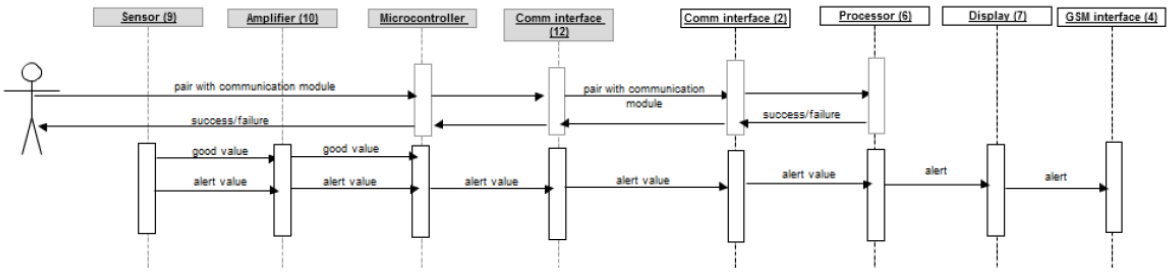

Fig. 3 - The sequence diagram of the system

The limited life span allows forgetting the inappropriate internal parameter settings ([11]). This may lead to short periods of recession, but it avoids long stagnation phases due to unadapted strategy parameters [13]. The $(\mu+\lambda)$ and (μ,λ) selection fit into the same formal framework with the only difference being the limited life time of individuals in (μ,λ) method.

E.Genetic parameters

The genetic parameters are very important for the success of a GA, equally important as the other aspects, such as the representation of the individuals, the initial population and the genetic operators. The most important parameters are:

- the population size μ has been set to 5 times the number of clusters. This turned out to be the best number of individuals in a generation.
- the intermediate population size λ was chosen twice the size of the population: $\lambda = 2 \cdot \mu$.
- mutation probability was set at 5%.

4. DIFFERENCES BETWEEN OUR SYSTEM AND ITS MAIN COMPETITOR

A very similar invention is the one described by the patent DE 10029065 [7], depicted in figure 4. The transmission unit (3) transmits measured values from a sensor to a communication terminal (1). The communication terminal is designed to display (8) and/or store (12) the measured values. A time measuring device (13) measures the time during the detection of the measured values. A computer unit (6) may output signals to a telephone number, e-mail address or output a text message to a telephone number, or output an audible, visual or vibration signal.

However there are several differences between the two. The first one consists of the existence of the microcontroller (11) in the sensory module. It can compare the values sensed by the sensor (9) with the normal ones and sends them to the communication equipment (1) only if there are significant variations. This way, an important energy is saved, especially in the case of wireless communication.

A second difference is that in our system, the GPS (5) is embedded into the communication equipment (1) and it is not external, as in the case of patent DE 10029065. So that, our model has 2 important modules (sensory and communication), whereas the one in the competitor patent has a third one - the GPS.

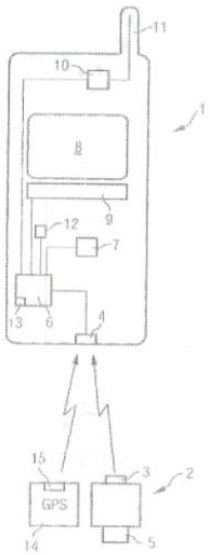

Fig. 4 - The system presented in patent DE 10029065[7]

4. CONCLUSION

The article presents a device, subject of the patent A 201100939, which monitors a patient's body parameters, such as pulse, heart rate and temperature and alerts when their values are out of regular ranges. The main advantages of the system are:

- the system is mobile, so that the patient can live her normal life, without having to stay all the time in a limited area, such as home, hospital etc.;
- the alerts emitted by the system contain also the coordinates of the patient;
- the communication between the sensory module and the communication module is done only when needed, not all the time;
- the communication module interfaces with a server side application, used by physicians, which can send a rescue team.
- low cost of the equipment;
- low cost of the maintenance.

A. Future work

Future developments of the solution presented in this article are possible, regarding both hardware and software functionalities. The usage of the device may be extended for monitoring the patient:

- in the acute phases of illnesses;
- for diagnosing specific illnesses;
- in post-operator stages.

In all these cases, specific devices are used, such as Holters [4], which act like portable EKGs, or electrocardiograms. An electrocardiogram interprets a heart's electrical activity over time. Patients commonly wear a Holter for a period of 24 hours, but if symptoms remain too intermittent to diagnose, doctors may require patients to wear the device for a longer period. The Holter records EKG readings on strips on a tape. After the Holter is removed, a physician can review the EKG results to analyze the heart rhythms. Therefore it would be very useful to connect the holter to our system and send the data real-time. Doing so, is something goes wrong with the patient, the physicians are informed and can intervene immediately.

Another improvement regards the possibility of the serverside application to take into account the capacities and facilities of the ambulances. In this cases, more complex algorithms are to be used, such as the ones presented in [8], [10].

ACKNOWLEDGEMENT

This work was supported by the Programmes POSDRU/173/6.1/S/148909 and POSDRU/168/6.1/S/144985, project co-funded from European Social Fund through the Human Resources Sectorial Operational Program 2007-2013.

REFERENCES

[1] T. Back, F. Hoffmeister and H. Schwefel, *A survey of evolution strategies,* in Proc. of the 4th International Conference on Genetic Algorithms, San Diego, CA, July, 1991, Morgan Kaufman.

[2] Henry-Labordere, *The record balancing problem: A dynamic programming solution of a generalized traveling salesman problem*, RAIRO Operations Research, B2, pp. 43-49, 1969.

[3] O. Matei, *Evolutionary Computation: Principles and Practices*, Risoprint, 2008.

[4] Arthur J. Moss, *Noninvasive electrocardiology: clinical aspects of Holter monitoring*, Springer, 2000.

[5] Patent RO 122960, *Sistem de monitorizare, teletransmisie si avertizare privind parametrii fiziologici vitali ai unor persoane expuse la factori de risc prin aceea ca activitatea lor se desfasoara in conditii extreme.*

[6] Patent RO 112575, *Sistem de teletransmisie si monitorizare a semnalelor biologice.*

[7] Patent DE 10029065, *Body function detector for monitoring pulse, blood pressure, etc., transmits measured values for display and storage on everyday communications terminal.*

[8] P.C. Pop, O. Matei, C. Pop Sitar and C. Chira, *A genetic algorithm for solving the generalized vehicle routing problem*, in Proc. of HAIS 2010,Part II, Editors E.S. Corchado Rodriguez et al., Lecture Notes in Artificial Intelligence, Springer, Vol. 6077, pp. 119-126, 2010.

[9] P.C. Pop, O. Matei and C. Sabo, *A New Approach for Solving the Generalized Traveling Salesman Problem,* in Proc. of HM 2010, Editors M.J. Blesa et al., Lecture Notes in Computer Science, Springer, Vol. 6373, pp. 62-72, 2010.

[10] P.C. Pop, O. Matei and H. Valean, *An Efficient Soft Computing Approach to the Generalized Vehicle Routing Problem*, Advances in Intelligent and Soft Computing, Springer, Vol. 87, pp. 281-289, 2011.

[11] Pop, Petrica C., and Oliviu Matei. "*An improved heuristic for the bandwidth minimization based on genetic programming*." *Hybrid Artificial Intelligent Systems*. Springer Berlin Heidelberg, 2011. 67-74.

[12] J. P. Saskena, *Mathematical model of scheduling clients through welfare agencies,* Journal of the Canadian Operational Research Society, Vol. 8, pp. 185-200, 1970.

[13] H.P. Schwefel, *Collective phenomena in evolutionary systems,* in Proc. of 31st Annual Meetting of the International Society for General System Research, pp. 1025-1033, 1987.

[14] Srivastava, S. S. S. Kumar, R. C. Garg, and P. Sen, *Generalized traveling salesman problem through n sets of nodes,* CORS Journal, Vol. 7, pp. 97-101, 1969.

TRANSIENT REGIMES OF THE THREE-PHASE POWER TRANSFORMERS

Olivian **CHIVER**, Liviu **NEAMT**, Eleonora **POP**, Cristian **BARZ,** Adina **POP VĂDEAN,** Paul Petrică **POP**

Electrical, Electronic and Computer Engineering Department, North University Center of Baia Mare, Technical University of Cluj-Napoca

olivian.chiver@cunbm.utcluj.ro

Keywords: Power transformer, finite elements, transient analysis.

Abstract*: The transient regimes of a three-phase power transformer will be studied in this paper. The transient currents in the windings will be determined both analytically and by finite elements method (FEM). The no load and short circuit regimes will be considered. The current dependence of the instantaneous phase voltage and of the initial current value will be highlighted, by FEM. In order to determine analytically the transient currents, for inductances the analytical and FEM values will be used. The inductances are determined with FEM through the simulation of experimental tests. With FEM, the transient currents will be determined using transient analysis. Finally, the FEM and analytical results will be compared and discussed.*

1. INTRODUCTION

The electricity consumption in the world increases permanently. The more stringent restrictions regarding the interruption of power supply or other power quality parameters are imposed by the quality standards. The entire system of generation, transmission and distribution of electricity must work interconnected in a predictable manner and often loaded near to the maximum capacity, in order to comply with these rules. It is obvious that understanding and predicting how the entire system behaves requires thorough knowledge of the behavior of the components, separately and then interconnected. The main elements of the

system are: generators, transformers and transmission lines. This paper is oriented toward power system transformers operating at power frequency level (50 Hz).

Generation of power with the synchronous machine is usually at a relatively low voltage, which is most desirable economically. Stepping up the voltage to high voltage, or extra high voltage, is done through power transformers to match the power transmission requirements: the minimization of the losses and the increase of the transmission power of the lines. The level of the transmission voltage is then stepped down (usually in many stages and of course using power transformers) for distribution and utilization purposes.

From technical-economical point of view, often more transformers must work in parallel. The connection or disconnection to or from the network depends on the electricity needs at a time. The no loaded transformer connection to the network determines a transient regime. The duration of the transient process and the manner in which the system is affected depends on the voltage, power and the circuit parameters of the transformer. The no load transient current is not dangerous for the transformer, but the transformer protection can be triggered.

When the sudden short circuit occurs, another transient regime arises. Although the duration of this regime is less than in the first case, the currents are well above the nominal value and the electrical loads are very important. The values of the transient currents, for different situations, must be accurately calculated in order to have a correct sizing of the protections. In this paper, the analytical results (of course based on simplified calculation) obtained using the value of electrical parameters analytically determined first, and then the values obtained by FEM simulations, will be discussed. Finally, the transient currents will be determined by transient finite elements analysis. In this case the variation of the inductances during the transient process is taken into account.

2. TRANSIENT REGIMES

2.1. Analytical solutions

In case of the no load connection to the network, the current variation in the primary winding of the transformer is described by equation (1). The resistive drop voltage is neglected and also the residual magnetic flux and the inductance is considered constant.

$$i_{10}(t) = -\frac{\sqrt{2}V_1}{\omega L_{10}} sin(\omega t + \alpha_{10} - \varphi_{10}) - \left(\frac{\sqrt{2}V_1}{\omega L_{10}} sin(\alpha_{10} - \varphi_{10} \right) \cdot e^{-R_{10}t/L_{10}} \quad (1)$$

In (1) is noted with: V_1 – the phase voltage; R_{10}, L_{10} – the phase resistance and inductance respectively, in no load regime; ω – the angular frequency; φ_{10} - the power factor in no load regime and α_{10} - the initial voltage phase in the connection moment.

In case of the sudden short circuit, the current variation is described by equation (2), where is noted: with $i_1(0)$ the initial current.

$$i_{1sc}(t)=\frac{\sqrt{2}V_1}{\sqrt{R_{sc}^2+(\omega L_{sc})^2}}sin(\omega t+\alpha_{sc}-\varphi_{sc})+\left(i_1(0)-\frac{\sqrt{2}V_1}{\sqrt{R_{sc}^2+(\omega L_{sc})^2}}sin(\alpha_{sc}-\varphi_{sc})\right)\cdot e^{-R_{sc}t/L_{sc}} \quad (2)$$

The other parameters have the same meaning as in (1), but for the short circuit regime.

For the analyzed power transformer, the inductance in no load and short circuit regime respectively, analytically computed, has the values 70.14 H and 0.244 H. Also for no load regime the resistance is 9.21 Ω, and the short circuit resistance is 19.7 Ω. The rated voltages are 10000/400 V.

2.2. FEM – Analytical solutions

In this case the previous relationship has been used, but for inductances the FEM computed values were inserted. In order to compute these inductances, the corresponding numerical models were built. The models contain the magnetic core (the yokes and the column), the electrical circuits (six coils) and the air volume surrounding the transformer, fig. 1. Because this is not a reduced model (the entire transformer is included) on the all boundary of the analyzed domain, ”Flux tangential” boundary conditions were used.

In order to compute the inductance for no load regime there are several possibilities, further the one used in this paper being described. The number of turns and resistance for each primary and secondary coil were set. Next, the primary winding was supplied for a three phase voltage source and the secondary winding is no loaded, fig. 2 (the no load test is simulated). After the time-harmonic analysis, the no load current phase was obtained and the corresponding inductance was computed.

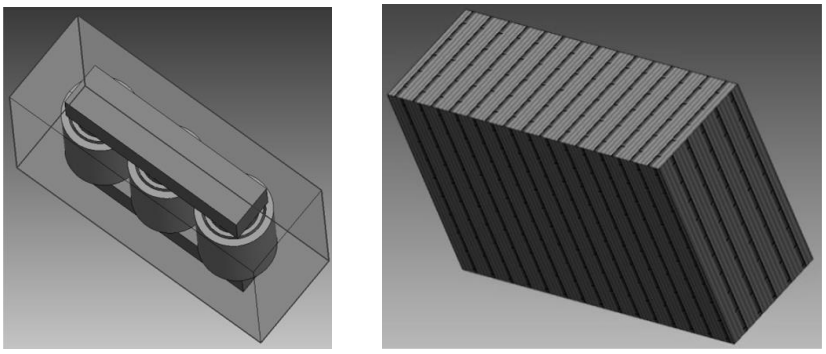

Fig. 1- The numerical model and the boundary condition

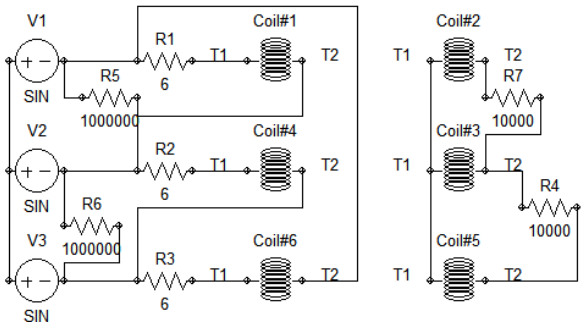

Fig. 2 – The winding feeding in no load regime

The studied transformer has delta connection in primary and wye connection in secondary. The R_1, R_2 and R_3 resistances are introduced to correct the resistance of each coil of the primary winding, so that the resistance be the same to the analytically computed one. The R_4, R_5, R_6 and R_7 resistances represent voltmeters.

The short circuit inductance can also be determined by FEM in several manners. In this paper it has been obtained simulating the short circuit test. With the secondary winding short circuited, fig. 3, the primary winding has been fed so that the current be the rated one. Time-harmonic analysis will be performed and the winding currents will be obtained. Based on the primary winding current, short circuit resistance and the phase voltage, the short circuit inductance will be computed. The R_8, R_9, and R_{10} resistances are in series with the secondary coils because in the numerical model, the insulated material is not taken into account and the model resistance is lower than the analytically computed one.

Based on FEM results, the inductance in no load regime is 69.34 H and the short circuit inductance is 0.188 H.

2.3. FEM solutions

In order to compute the transient currents by FEM, a transient analysis will be performed. The numerical model is the same with the former one, but switches are inserted in the electrical circuits, fig. 4, and they close at a preset time.

So for no load connection to the network, in primary winding three switches are used (S_1, S_2, S_3). For sudden short circuit, two switches are used (S_4 and S_5) in secondary winding.

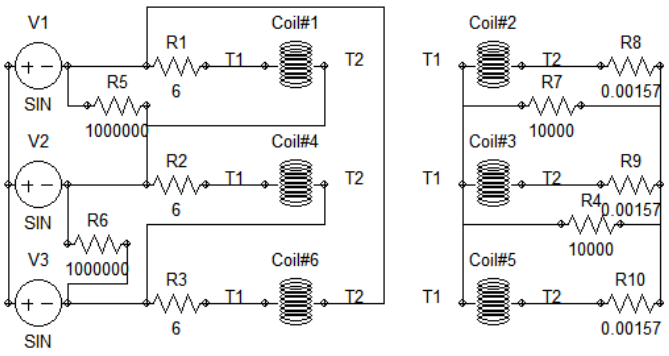

Fig. 3 – The winding feeding at short circuit test

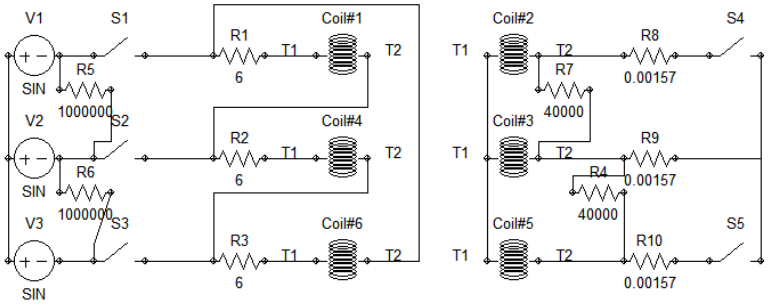

Fig. 4 – The winding of transformer in transient simulation

In transient analysis the used step was 1 ms. The total analysis time was 1 s for no load connection to the network and 0.4 s for sudden short circuit.

3. RESULTS

For the two transient regimes, the obtained results (analytical, FEM – Analytical and transient FEM) are showed in the following.

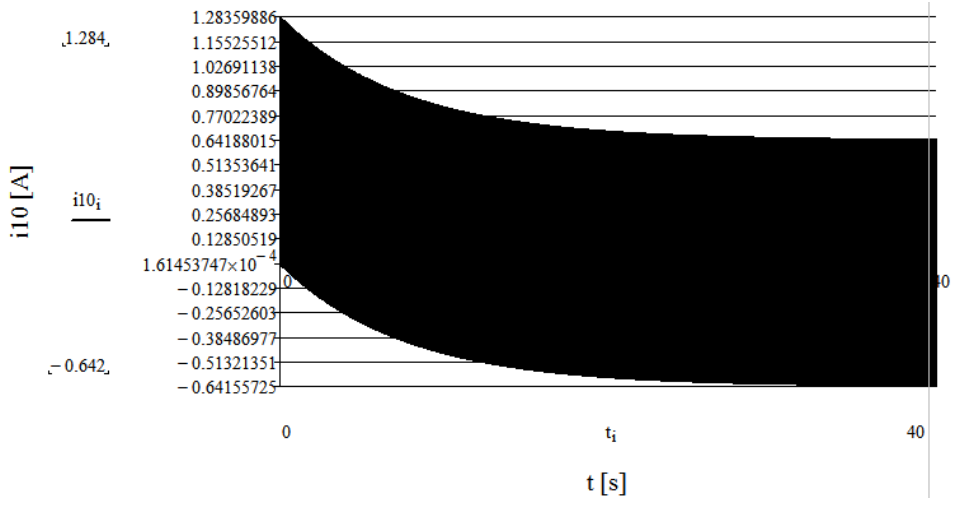

a)

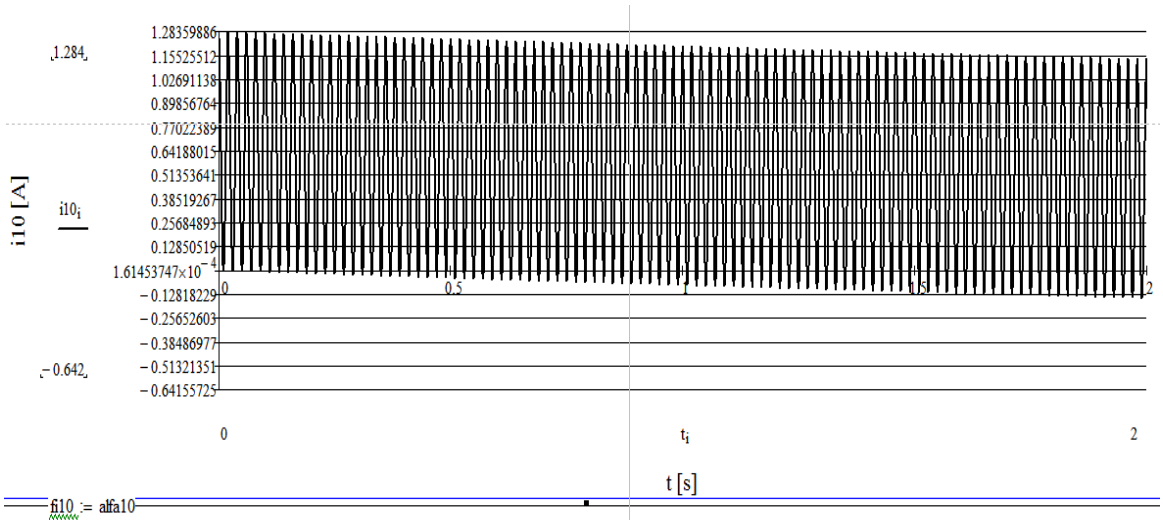

b)

Fig. 5 – The transient current for no load connection to the network: a) (0-40s) and b) (0-2s); α_{10}=0. Analytical results

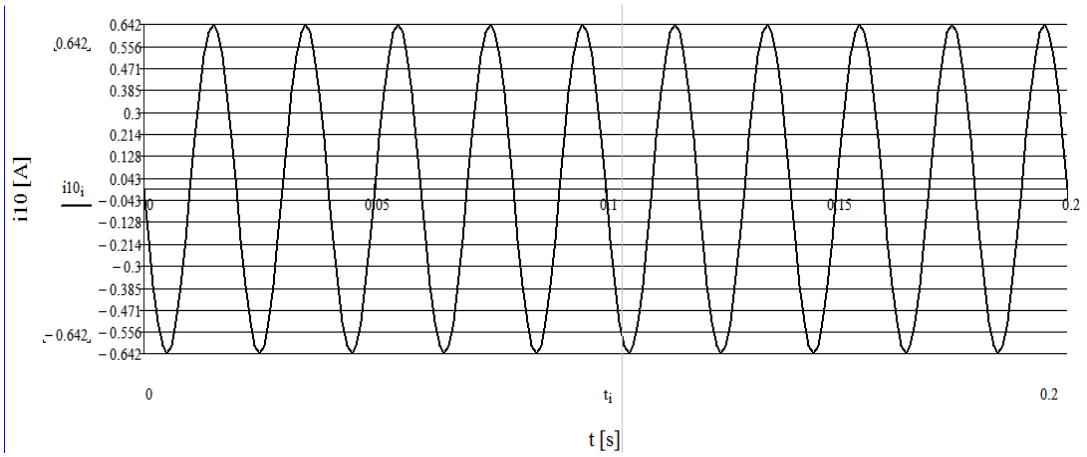

Fig. 6 – The current for no load connection to the network: (0-0.2s); $\alpha_{10}=\varphi_{10}$. Analytical result

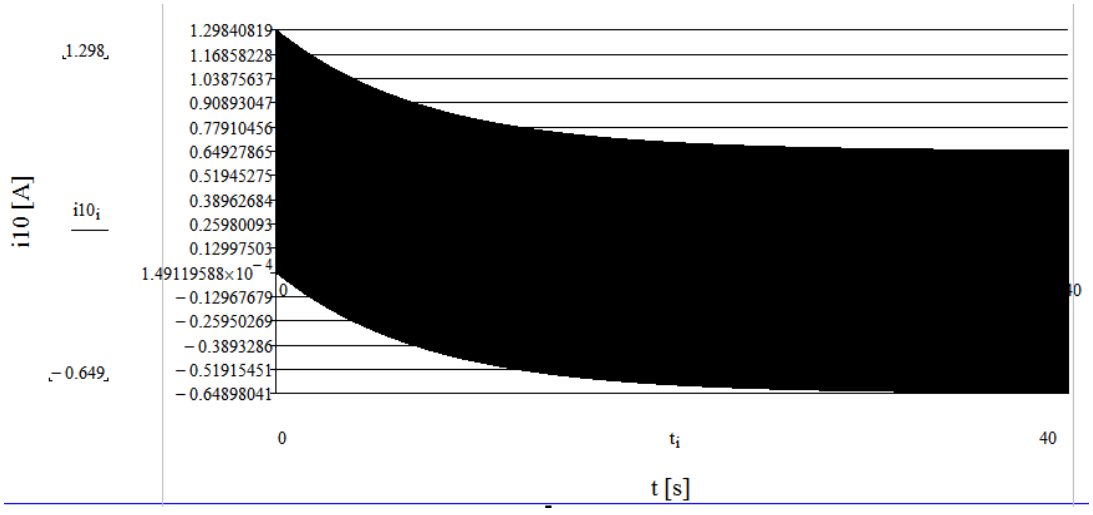

a)

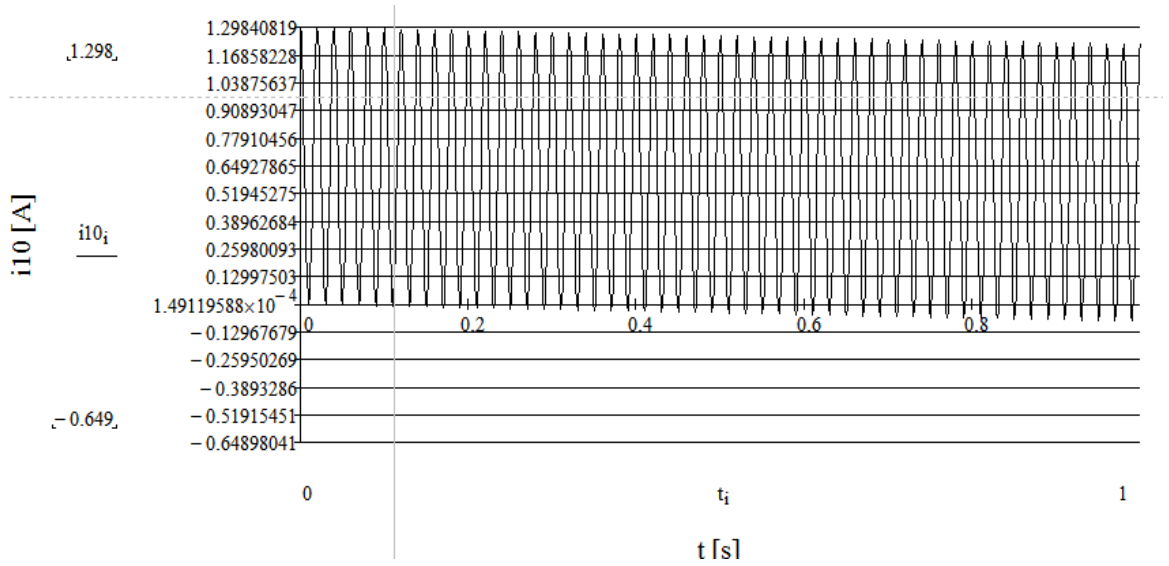

b)

Fig. 7 – The transient current for no load connection to the network: a) (0-40s) and b) (0-1s); α_{10}=0. FEM - Analytical results

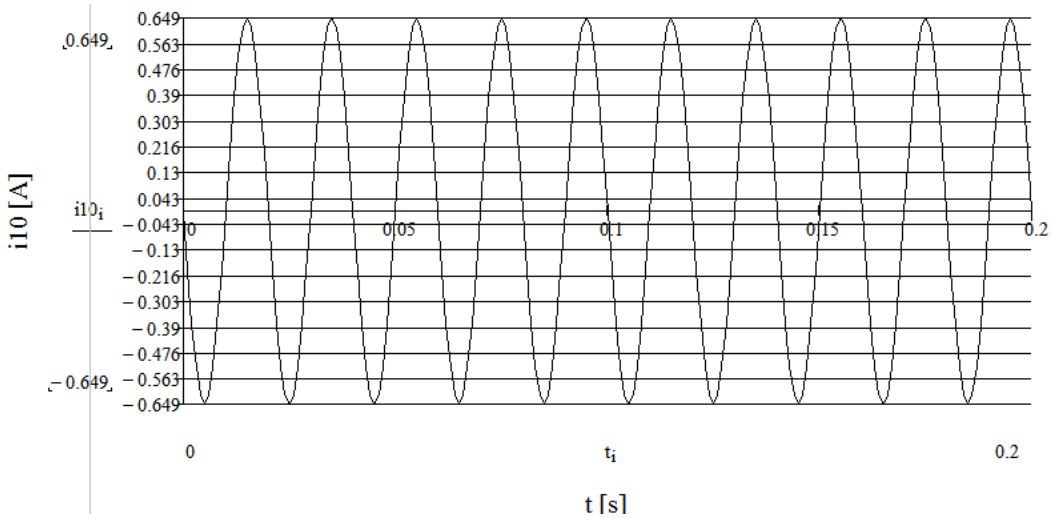

Fig. 8 – The current for no load connection to the network, (0-0.2s); $\alpha_{10}=\varphi_{10}$. FEM - Analytical result

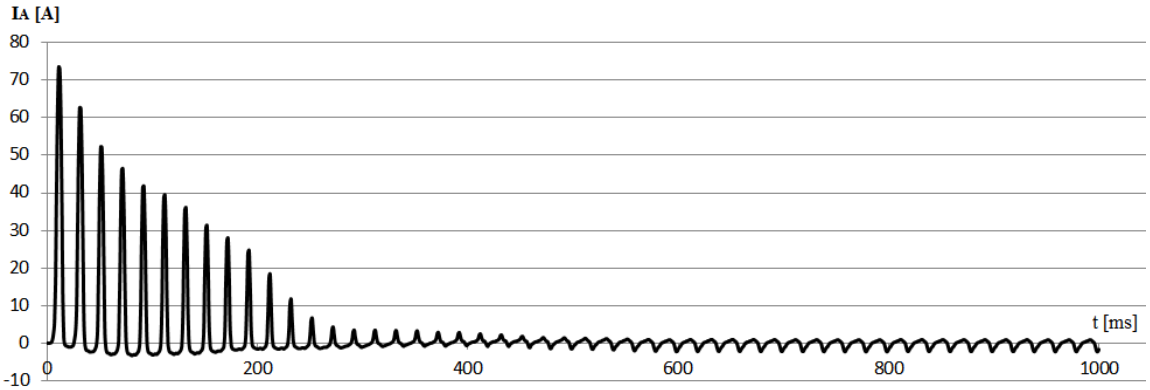

a) 0-1000 ms

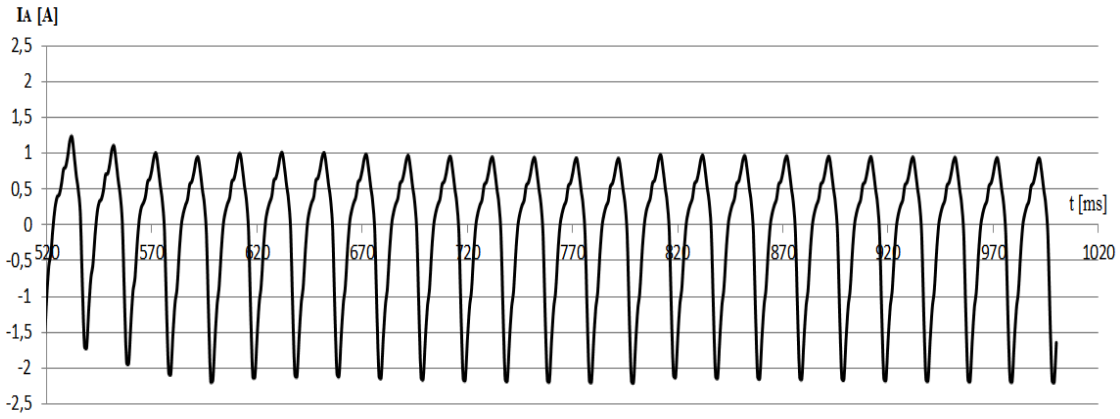

b) 520-1000 ms

Fig. 9 – The transient current for no load connection; α_{10}=0; FEM result

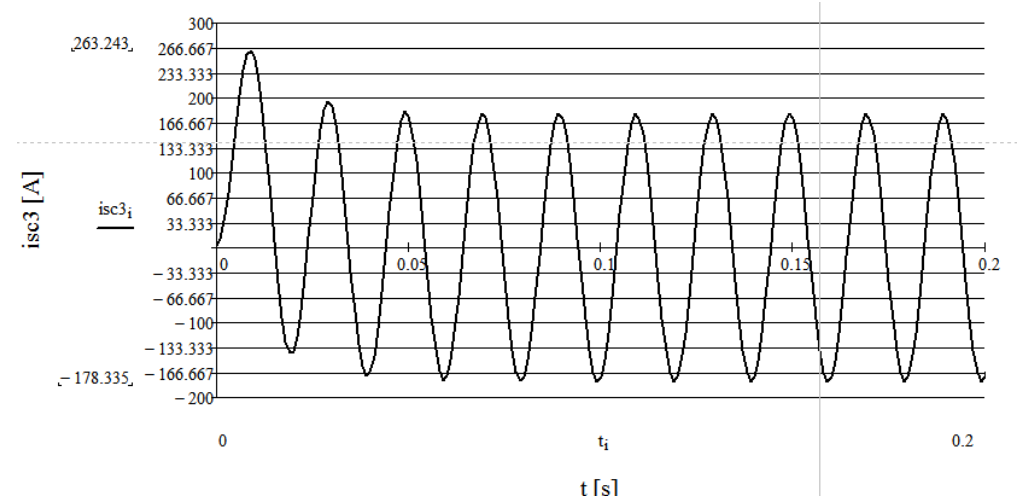

a)

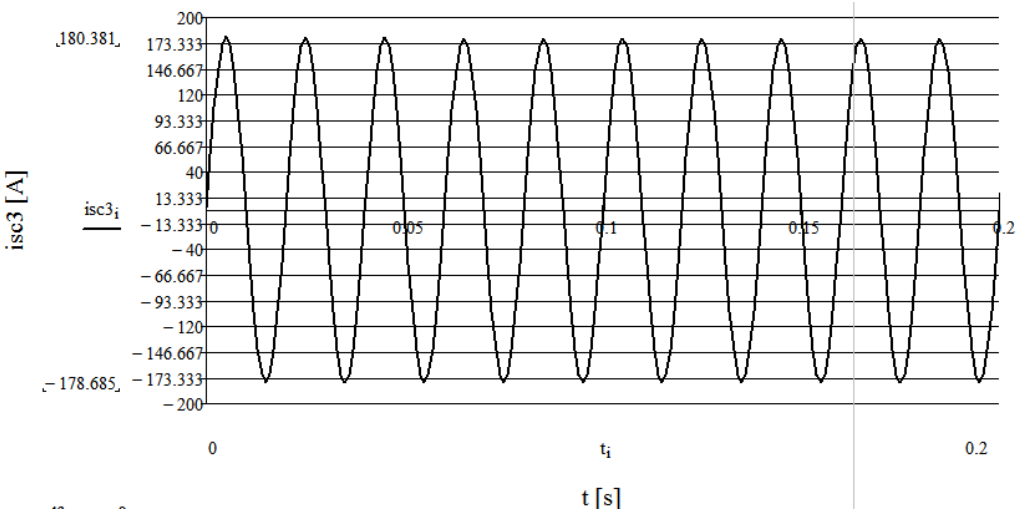

b)

Fig. 10 – The current for sudden short circuit; a) α_{sc}=0; b) α_{sc}=φ_{sc}. Analytical results

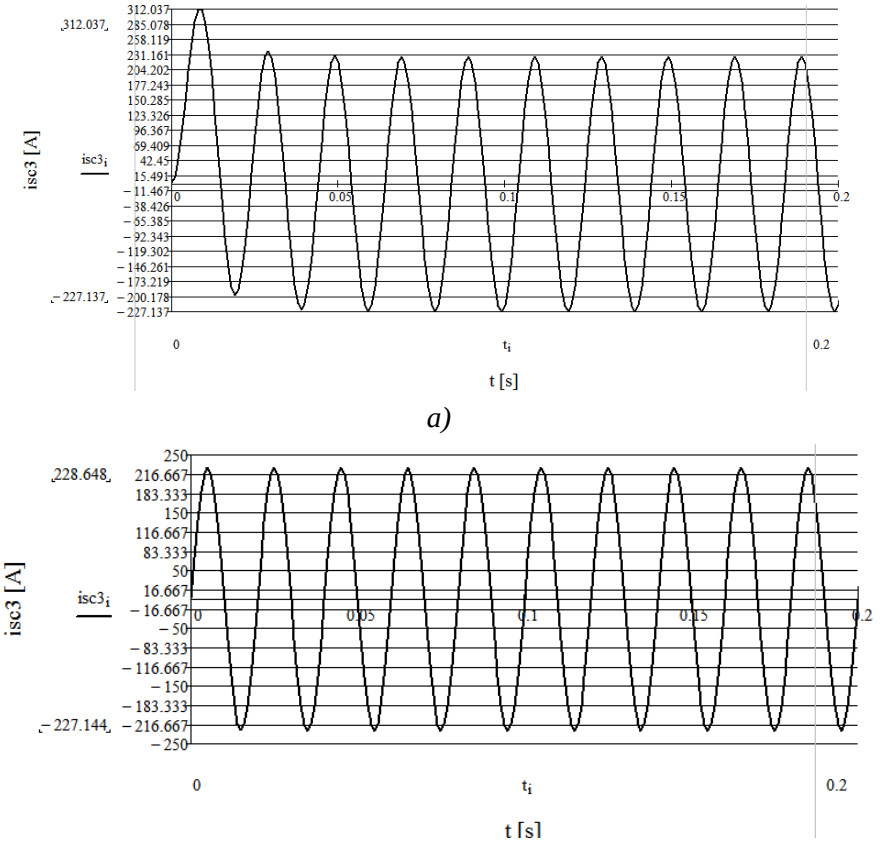

Fig. 11- The current for sudden short circuit: a) $\alpha_{sc}=0$; b) $\alpha_{sc}=\varphi_{sc}$. FEM - Analytical results

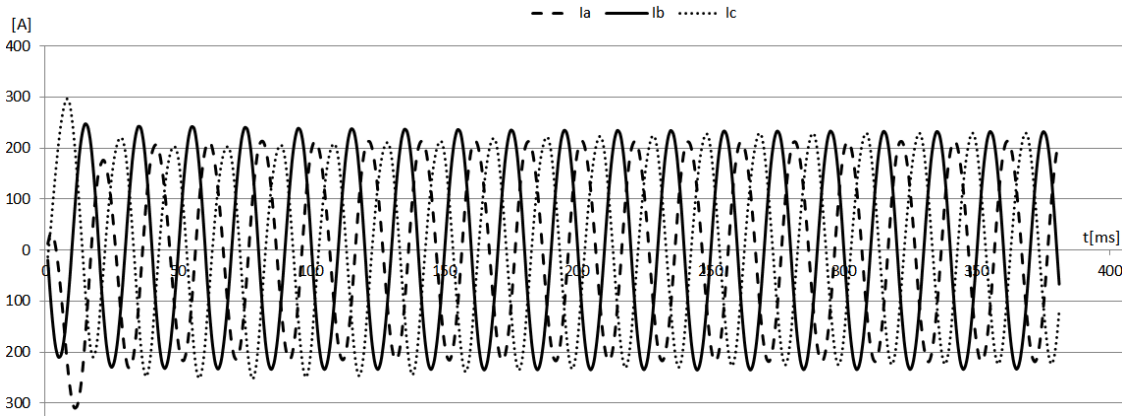

Fig. 12 – The transient currents for sudden short circuit; FEM solutions

4. CONCLUSIONS

Regarding the obtained results, it can be noticed that for the inductance in no load regime, the analytical value is very close to the FEM value. For this reason, the transient current in case of no load connection to the network, analytically computed, has the same maximum value as the FEM – Analytical one. As concerning the current obtained by transient analysis, it differs very much from the previous ones. This maximum value is approximately 73 A, that means over 100 times the value of the steady states current, being in accordance with specialty literature [3]. It can be emphasized that in case of no load connection to the

network, the considered simplifying hypotheses lead to unacceptable errors, even if the used values for the transformer parameters are FEM computed. The main cause of these errors is that the inductance value has been considered constant. Actually this inductance has a low initial value and then increases up to the steady state value. For the studied transformer, it has been noticed that the initial value is only 1.23 H and the steady state value is 69.34 H, which means that the initial value is more than 50 times lower than the steady state value.

As for short circuit, the FEM inductance mainly differs from the analytical one. This is because the magnetic core material used in simulation has, in linear domain, the magnetic properties a little different from those used in analytical computation. On the other hand, the transient current FEM – Analytical determined is very close to the current obtained by transient FEM. This is due to the fact that short circuit inductance is actually constant, because the magnetic core is slightly loaded, working on the linear B-H characteristic.

REFERENCES

[1]. N. Bianchi, *Electrical machine analysis using finite elements*, CRC Press, Taylor & Francis Group, 6000 Broken Sound Parkway NW, Suite 300, 2005.

[2]. K. J. Binns, P. J. Lawrenson, C. W. Trowbridge, *The analytical numerical solution of electric and magnetic fields*, Pergamon Press, Oxford, 1963.

[3]. A. Câmpeanu, I. Vlad, Mașini electrice. Teorie, încercări și simulări, Editura Universitaria Craiova, 2008.

[4] O. Chiver, L. Neamt, M. Horgos, S. Oniga, A. Buchman, *The Study of Transient Regimes for a Shell-Type Transformer*, Carpathian journal of electronic and computer engineering, ISSN 1844 - 9689 Vol.4/nr.1/2011;

[5]. I. Cioc, I. Vlad, G. Calotă, *Transformatorul electric. Construcție. Teorie. Proiectare. Realizare. Exploatare*, Editura Scrisul Românesc, Craiova, 1989.

[6]. V. Fireţeanu, M. Popa, T. Tudorache, *Modele numerice în studiul și concepția dispozitivelor electrotehnice*, Ed. Matrix Rom, Bucureşti, 2004.

[7]. M. Gyimesi, D. Ostergaard, *Inductance computation by incremental finite element analysis*, IEEE Transactions on Magnetics, vol. 35, no. 3, May 1999.

[8]. K.Karsai ,D.Kerenyi and L.Kiss, *Large power transformers*, Hungary, Elsevier, 1987.

[9]. A. Naderian-Jahromi, Jawad Faiz and Hossein Mohseni, *Calculation of distribution transformer leakage reactance using energy technique*, Australasian Universities Power Engineering Conference, AUPEC 2002.

[10]. P. P. Silvester, R. L. Ferrari, *Finite elements for electrical engineers* - Second edition, Cambridge University Press, 1990.

[11]. J.Turowski, M.Turowski and M. Kopec, *Methods of three-dimensional network solution of leakage field of three-phase transformers*, IEEE Transactions on Magnetics, Vol. 26, No. 5, September 1990, pp. 2911-2919.

INSTRUCTIONS FOR AUTHORS

Name **SURNAME**[1], Name **SURNAME**[2], **...**

[1] *Affiliation of 1st author,* [2] *Affiliation of 2nd author, ...*

Email of 1st author, Email of 2nd author, ...(it is compulsory only for the first author)

Keywords: List 3-4 keywords *(aligned to the left, 10 pt. bold; please choose keywords from IEEE Approved Indexing Keyword List)*

Abstract: *Abstract of max. 120 words, justify, 10 pt. regular.*

1. INTRODUCTION

The paper must be written in English. It shall contain at least the following chapters: introduction, research course (mathematical algorithm); method used; results and conclusions, references.

Use DIN A4 Format (297 x 210 mm) MSWord format. Margins: top, bottom, left and right 2.5 mm each. The text should be written on one side of the page only. Use Times New Roman fonts, line spacing 1.3. The font formats are: paper title: 14 pt bold italic, capital letters, author's name(s): 12 pt regular for name and 12 pt. bold, for surname; Affiliation: 11 pt. italic; key words: 10 pt, bold; Abstract: 10 pt. italic, word Abstract in 10 pt. bold; chapter titles (do not use automatic numbering): 12 pt bold, capital letters; subtitles: 12 pt bold lower case letters; body text: 12 pt. regular. tables and figures caption: 11 pt. italic; references: author 11 pt. bold, title 11 pt. italic, year, pages, ... in regular.

The number of pages is not restricted.

2. FIGURES AND TABLES

Figures have to be made in high quality, which is suitable for reproduction and printing. Don't include photos or color prints if there are not clearly intelligible in gray scale

option. Place figures and tables at the top or bottom of a page wherever possible, as close as possible to the first reference to them in the paper. Use either *fig. 1* or *figure 1* when necessarily.

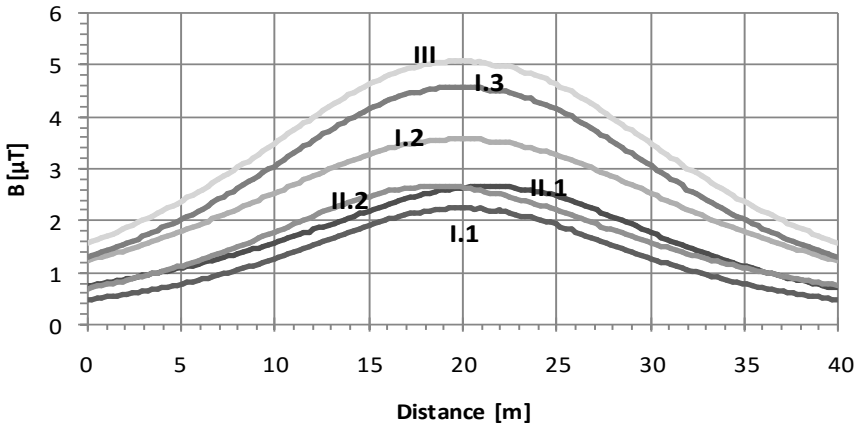

Fig. 4 - Magnetic flux density at 1 m above the ground

Table 1. Transposing principle

	Circuit											
	1	*2*	*1*	*2*	*1*	*2*	*1*	*2*	*1*	*2*	***1***	***2***
1/3	*R*	*T*	***R***	***R***	*R*	*S*	*R*	*T*	*R*	*S*	***R***	***R***
line	***S***	***S***	*S*	*T*	*S*	*R*	*S*	*R*	*S*	*T*	***S***	***S***
length	*T*	*R*	*T*	*S*	***T***	***T***	*T*	*S*	*T*	*R*	***T***	***T***
1/3	*T*	*S*	***T***	***T***	*T*	*R*	*T*	*S*	*T*	*R*	***T***	***T***
line	***R***	***R***	*R*	*S*	*R*	*T*	*R*	*T*	*R*	*S*	***R***	***R***
length	*S*	*T*	*S*	*R*	***S***	***S***	*S*	*R*	*S*	*T*	***S***	***S***
1/3	*S*	*R*	***S***	***S***	*S*	*T*	*S*	*R*	*S*	*T*	***S***	***S***
line	***T***	***T***	*T*	*S*	*T*	*S*	*T*	*S*	*T*	*R*	***T***	***T***
length	*R*	*S*	*R*	*T*	***R***	***R***	*R*	*T*	*R*	*S*	***R***	***R***
Name	***I.1***		***I.2***		***I.3***		***II.1***		***II.2***		***III***	

3. EQUATIONS

Equations are centred on page and are numbered in round parentheses, flush to right margin. In text respect the following rules: all variables are italic, constants are regular; the references are cited in the text between right parentheses: [1], the list of references has to be arranged in order of citation.

REFERENCES

[1]. International Commission on Non-ionizing Radiation Protection, *Guidelines for limiting exposure to time-varying electric, magnetic and electromagnetic fields (Up to 300 GHz)*, Health Physics, vol. 74, no. 1, pp. 494-522, 1998.

[2]. A. Marincu, M. Greconici, *The electromagnetic field around a high voltage 110 KV electrical overhead lines and the influence on the biological systems,* Proceedings of the 5th International Power Systems Conference, pp. 357-362, Timisoara, 2003.

[3]. Gh. Hortopan, *Compatibilitate electromagnetică*, Ed. Tehnică, 2005.